

The nature of late-type spiral galaxies: structural parameters, optical and near-infrared colour profiles, and dust extinction

Katia Ganda¹, Reynier F. Peletier^{1*}, Marc Balcells² and Jesús Falcón-Barroso³

¹*Kapteyn Astronomical Institute, Postbus 800, 9700 AV Groningen, The Netherlands*

²*Instituto de Astrofísica de Canarias, Vía Lactea s/n, 38700 La Laguna, Tenerife, Spain*

³*European Space Agency / ESTEC, Keplerlaan 1, 2200 AG Noordwijk, The Netherlands*

Released 2009 Xxxx XX

ABSTRACT

We analyse V and H -band surface photometry of a sample of 18 Sb-Sd galaxies. Combining high resolution HST images with ground-based NIR observations, we extract photometric profiles, which cover the whole disk and provide the highest possible resolution. This is the first photometric study of late-type spirals for which the stellar kinematics have been measured. For 10 out of the 18 galaxies, HST data in both F160W (H) and F606W (V) are available, and, for those, we present colour maps and radial colour profiles at the resolution of the Hubble Space Telescope.

Colours vary significantly from galaxy to galaxy, but tend to be highly homogeneous within each galaxy, with smooth and flat colour profiles. Some of the colour maps show jumps in the inner regions, likely due to dust. We determine extinction-maps in an almost model-independent way using the $V - H$ colour map and the SAURON Mg b absorption line map of Ganda et al. (2007). The maps show that A_V ranges from 0 to 2 mag, in the center from 0 to 1.5 mag, in agreement with the models of Tuffs et al. (2004).

We describe the surface brightness profiles as the superposition of an exponential disk and a Sérsic bulge. The bulges are small (0.1-2.5 kpc), and show a shape parameter n ranging from ≈ 0.7 to 3, with a mean value smaller than two: well below the value for the *classical* de Vaucouleurs bulges. Most galaxies (16 out of 18) show a central light excess above the Sérsic fit to the bulge, which can be interpreted as a nuclear cluster, as shown by previous studies. We provide zero-order estimates for the magnitude of these components. We discuss the correlations among the structural galaxy parameters and with other relevant quantities such as Hubble type and stellar velocity dispersion. We compare these results with a recent paper by Graham & Worley (2008), who present a summary of most of the near-IR surface photometry of spirals in the literature. For both early and late type spirals, bulge luminosity strongly correlates with central velocity dispersion; at constant velocity dispersion, later-type bulges are larger and less dense, and have lower Sérsic n values.

Key words: galaxies: bulges - galaxies: evolution - galaxies: formation - galaxies: photometry - galaxies: spiral - galaxies: structure

1 INTRODUCTION

It has been known for many years that the inner regions of spiral galaxies are fundamentally different from their outer parts. The inner parts are generally rounder, redder, and show a higher fraction of random vs. ordered motion. Images of spirals show that less star formation is present in the central regions. Radial surface brightness profiles can be fitted well by a large exponential disk and a central, steeper component (e.g., Kent 1984). When looking at the stellar kinematics, one finds that v/σ in the inner parts is much lower than in the outer parts, where the rotation velocity is high

and the stellar dispersion low (e.g., Noordermeer 2006). As a result, people traditionally viewed spiral galaxies as a combination of a flattened disk and a spheroidal central component called ‘bulge’, which are assumed to be physically and dynamically different: in this picture, the disk component is rotationally supported against gravity, and the bulge is a hotter system, similar to an elliptical galaxy. To understand how spiral galaxies are built, one generally does a bulge-disk decomposition and studies the parameters of both components. If one wants to go into more details, one can go one step further, and also study possible components such as bars, spiral arms, rings, and inner disks (see for example de Jong 1996a, Prieto et al. 2001 and Erwin & Sparke 2002).

* E-mail: peletier@astro.rug.nl

When doing the bulge-disk decomposition, it is imperative

that the decomposition is well-defined. The bulge-disk decomposition can be based e.g. on the surface brightness profile (photometric decomposition), the stellar kinematics (kinematic decomposition) or on the two-dimensional axis ratio (morphological definition) (see Peletier 2008). The physical interpretation of the resulting parameters then depends strongly on the definition. Up to now most B/D decompositions have used the photometric decomposition, using a one-dimensional azimuthally averaged surface brightness profile. Such profiles can generally be fitted well by an exponential disk and a central Sérsic $r^{1/n}$ distribution (Andredakis, Peletier & Balcells 1995, Graham 2001). The Sérsic index n has been found to correlate with the morphological type of the galaxy, and generally ranges between 1 and 4. For a comprehensive review about the Sérsic index see Graham & Driver (2005). In recent years it has been discovered that the bulges with surface brightness profiles that are close to exponential (i.e. Sérsic index close to 1) are different from bulges with larger Sérsic indices, which resemble more elliptical galaxies. Bulges with exponential profiles appear to contain more dust, show more recent star formation, are more flattened and more rotationally supported (Kormendy 1992, Kormendy & Kennicutt 2004, Fisher & Drory 2008). These objects are called pseudo-bulges, but one might also call them central disks. For more detailed examples and references we refer the reader to the comprehensive review by Kormendy & Kennicutt (2004), which presents a complete summary of observational evidence for this kind of bulge and their formation via secular evolution: bulges could result from the evolution of disk dynamical instabilities. Numerical simulations seem in fact to suggest that the dissolution of bars inside the disks may trigger the formation of three-dimensional stellar structures with roughly exponential profiles (Pfenniger & Norman 1990, Combes et al. 1990, Raha et al. 1991, Norman, Sellwood, Hasan 1996). It is also known that these processes are more effective in late-type galaxies rather than in early-types, despite the fact that there are examples of pseudobulges in Sa and even S0 galaxies (Erwin et al 2003, Kormendy & Kennicutt 2004). In this paper, we will also adopt the photometric bulge-disk decomposition.

Our purpose in this paper is to investigate the nature and interconnection of disks and bulges in a class of rather poorly studied objects: late-type spiral galaxies, full of dust and star forming regions, and characterised by relatively low-surface brightness; in the last years, galaxies towards the end of the Hubble sequence have been the target for a number of HST-based imaging surveys (Carollo et al. 1997, Carollo & Stiavelli 1998, Carollo, Stiavelli & Mack 1998, Carollo 1999, Carollo et al. 2002, Böker et al. 2002, Laine et al. 2002) which revealed the presence of a variety of structures in their inner regions: bulges, nuclear star clusters, stellar disks, small bars, double bars, star forming rings, whose formation and evolutionary patterns are not properly understood yet. Because of the extinction, a photometric analysis based on near-infrared data gives more reliable results (A_H is roughly a factor 8 lower than A_V ; Rieke & Lebofsky 1985). Another advantage of working in the NIR is that the NIR light is much less affected by recent episodes of star formation than optical light, and traces the old stellar populations hosting most of the luminous mass of galaxies. For the analysis of HST-NICMOS data the problem is, however, that the field of view is very small (about $20'' \times 20''$ for NIC2, so that an accurate determination of the sky background is very difficult. Here we use data from the 2MASS survey to solve this problem.

The sample that we study here is special, in that accurate stellar kinematic maps, stellar absorption line maps of a few strong lines, as well as emission line strengths of [OIII] and $H\beta$ have been determined, making it possible for us to study the relation between

structural parameters and stellar populations, the behaviour of ionized gas and the stellar potential. These maps come from SAURON (Bacon et al. 2001) integral field spectroscopy. The stellar and gas kinematics has been published in Ganda et al. (2006), while the absorption line maps have been analyzed in Ganda et al. (2007). Our sample of late-type galaxies can be easily compared to the early-type spirals of the SAURON Survey (de Zeeuw et al. 2002), presented in Falcón-Barroso et al. (2006) and Peletier et al. (2007). The fact that kinematic parameters are available for this sample makes it possible to study the position of late-type spirals on the $M_{Bulge} - \sigma$ relations, establishing in this way whether these bulges are similar in structure and formation to bulges of early-type spirals.

Given the renewed interest in the extinction in spiral galaxies (Driver et al. 2007, Graham & Worley 2008, hereinafter GW) we decided to use the unique property of this sample that the amount of extinction can be calculated by combining absorption line maps, which are basically independent of extinction, with broad band colour maps, such as the Mg b maps, which are affected by it. To do this, we determined high resolution $V - H$ maps for the 10 galaxies for which HST-F606W (V) images were available, in addition to F160W (H). The combination of colour and line strength gives the colour excess E_{V-H} in a model-independent way, which can easily be converted to A_V . This method is in principle very powerful, but has not been applied much in the literature, because of the lack of well-calibrated line strength data.

The paper is structured as follows. Section 2 describes the sample selection; Section 3 the photometric profiles and the methods applied for their extraction; Section 4 the actual bulge-disk decomposition; Section 5 compares the photometry in the NIR with the optical $V -$ band, and presents extinction maps; Section 6 investigates the correlations between the structural parameters and other galaxy properties; Section 7 addresses the frequent presence of inner additional components, and, finally, Section 8 summarizes the main results.

2 THE SAMPLE

The sample of galaxies on which we perform our bulge-disk decomposition is the same for which we presented the two-dimensional kinematical maps from SAURON integral-field spectroscopy in the paper by Ganda et al. (2006) and the line-strengths maps in the paper by Ganda et al. (2007).

The galaxies were optically selected ($B_T < 12.5$, according to the values given in de Vaucouleurs et al. 1991, hereafter RC3) with HST imaging available from WFPC2 and/or NICMOS. Their morphological type ranges between Sb and Sd, following the classification given in NED (from the RC3). Galaxies in close interaction and Seyferts were discarded. The resulting sample contains 18 nearby galaxies, whose properties are listed and illustrated respectively in Table 1 and Fig. 1 in Ganda et al. (2006).

3 PHOTOMETRIC PROFILES

3.1 Datasets used

We constructed surface brightness profiles for all galaxies combining datasets with different spatial resolution and field of view. We started from the $H -$ band images from the Two-Micron All Sky Survey (hereafter, 2MASS). Since these data do not have a sufficient spatial resolution for our purposes (2-3''; the pixel scale of

the 2MASS images retrieved from the archive is $1''$), we complemented the photometric profiles extracted from the 2MASS images with profiles extracted from NIR HST images (F160W), available for 11 out of 18 cases (marked with a single or double dagger in Table 1). To improve the spatial resolution at small radii for the remaining galaxies we used optical HST images (F814W, corresponding to the I -band). Since, on the other hand, 2MASS is rather shallow (reliable profiles can be extracted out to $\approx 5 - 8$ kpc for most of our galaxies), we needed an additional dataset for the outer parts, so that the disk geometry could be determined unambiguously, and an accurate sky level could be determined. For this reason, we decided to complement the profiles also with profiles extracted from infrared¹ images from the Digitized Sky Survey (hereafter, DSS), which are very deep, and therefore radially very extended. This also allows us a more accurate determination of the sky background. The DSS, 2MASS and NICMOS images downloaded from the archives were fully reduced, so we did not apply any further processing; as for the WFPC2-F814W images, we first created a mosaic from the four chips in order to maximize the field of view, using the IRAF task WMOSAIC in the STSDAS.HST_CALIB.WFPC package, rotated the resulting image to orient it to North up-East left and performed cosmic rays removal, using the IRAF tasks CRREJ and LACOS_IM, created by Pieter van Dokkum and available via his website².

3.2 Ellipse fitting

As a first step, we extracted the photometric profiles from the DSS images using the IRAF task ELLIPSE in the STSDAS.ANALYSIS.ISOPHOTE package, which fits elliptical isophotes to galaxy images, implementing the method initially described by Kent (1983, 1984) and Jedrzejewski (1987). We masked out bad pixels and foreground stars, but did not exclude dust lanes and star forming regions from the fitting. We first fitted ellipses to the images with the centre, position angle and ellipticity left as free parameters. In this way we obtained profiles of the centre coordinates; from these profiles we established the position of the centres, kept fixed in the following steps. In case of ambiguity, the centre was determined using isophotes at intermediate radii, since the very central ones can be affected by dust obscuration, and, in the particular case of the DSS images, by the seeing (or even by saturation of the images, in the worst cases).

We then fitted again ellipses to the images with the centre fixed at the chosen position and ellipticity and position angle free. From this second step we determined single values for the geometric parameters. In many cases in the outer parts of the galaxies, outside the nuclear region, the position angle and ellipticity converge to more or the less constant values. In other cases the situation is more complicated, especially for galaxies that are almost round, and there we picked the values that looked more reasonable at a visual inspection of the shape of the isophotes in the images.

Table 1 lists the position angles and ellipticities of our sample galaxies, together with some other basic data, and shows that in most cases the chosen values are very close to the values tabulated in the literature (mainly in the RC3); the cases which present the biggest discrepancies are actually galaxies almost face-on and/or

NGC (1)	Type (2)	M_B (3)	d (4)	Scale (5)	PA (6)	ϵ (7)	PA_{lit} (8)	ϵ_{lit} (9)
488†	3.0	-21.71	32.1	156	5	0.23	15	0.260
628†	5.0	-20.29	9.8	47	25	0.19	25	0.088
772†	3.0	-22.23	35.6	173	126	0.34	130	0.411
864†	5.0	-20.54	21.8	106	26	0.32	20	0.241
1042	6.0	-19.83	18.1	88	174	0.29	43	0.224
2805	7.0	-20.75	28.2	137	125	0.24	125	0.241
2964†	4.0	-19.74	20.7	100	96	0.45	97	0.451
3346	6.0	-18.89	18.9	92	100	0.16	111	0.129
3423	6.0	-19.54	14.7	71	41	0.23	10	0.149
3949†	4.0	-19.60	14.6	71	122	0.36	120	0.425
4030†	4.0	-20.27	21.1	102	37	0.24	27	0.276
4102†	3.0	-19.38	15.5	75	42	0.445	38	0.425
4254†	5.0	-22.63	19.4	94	50	0.27	62	0.129
4487	6.0	-19.12	14.7	71	77	0.37	75	0.324
4775	7.0	-19.81	22.5	109	96	0.135	52	0.067
5585‡	7.0	-18.32	8.2	40	38	0.36	30	0.354
5668	7.0	-19.65	23.9	116	120	0.155	164	0.088
5678†	3.0	-21.30	31.3	152	5	0.475	5	0.51

Table 1. Column (1): NGC identifier; column (2): morphological type (RC3); column (3): absolute blue magnitude, from HyperLeda, computed using distance in Mpc given in column (4); column (5): scale in pc/arcsec; columns (6) and (7): adopted position angle (PA) and ellipticity (ϵ) for the measurement of the photometric profiles (N–E); columns (8) and (9): position angle and ellipticity values tabulated in the literature (PA_{lit} and ϵ_{lit}); we refer to the RC3 values, with the exceptions of NGC 1042, 3346, 4254, 4775, 5668, where the angle is taken from Grosbøl (1985). The galaxies marked with a single or double dagger are those for which we used NICMOS imaging from the NIC2 or NIC3 cameras, respectively. For the remaining galaxies WFPC2-F814W images are available.

very round, for which the errors on the geometric parameters are in any case big. Once we had determined the geometric parameters, using ELLIPSE again we measured the intensities at each radius with centre coordinates, position angle and ellipticities fixed for all ellipses. From the resulting photometric profiles we subtracted then a value for the sky background estimated on the outer parts of the images. Following this, we fitted ellipses to the 2MASS images, with all the geometric parameters (centre coordinates, position angle and ellipticity) free and determined the centre coordinates in the same way as done for the DSS images. And after this we measured the intensity profiles, fixing the centre coordinates to the values just determined and the position angle and ellipticity to the values determined on the basis of the DSS profiles and subtracted an estimated value for the sky brightness. An analogous procedure was repeated for the NICMOS images, when available, and for the WFPC2-F814W images, in the cases where NICMOS was missing (see Table 1).

3.3 Combining the profiles

At the end of this procedure, for each galaxy we combined the three photometric profiles, to get a single profile with the maximum radial extension and spatial resolution allowed by the data. To do this, we first combined the profiles extracted from the DSS and 2MASS images, aligning them at the 2MASS level, and transformed the resulting ‘ground-based’ profile to an absolute magnitude scale using the zero point calibration (the keyword MAGZP) of the 2MASS images. For the 11 galaxies with available NICMOS imaging, we first calibrated independently the NICMOS profile to the absolute

¹ We used POSS-II Near-IR IVN+RG9 images, obtained from http://archive.stsci.edu/cgi-bin/dss_form/; the selected filter is close to the Z -band.

² <http://www.astro.yale.edu/dokkum/lacosmic/>

H (Vega) magnitude scale using the F160W zero points of 21.826 (plus a term taking into account the pixel scale) for the 10 galaxies with NIC2 data and 21.566 for NGC 5585, observed with NIC3, and then joined them with the calibrated ‘ground-based’ profiles; the quality of the matching of the two profiles gave us an indication of the quality of our estimation of the sky background in the HST image, which was then changed iteratively until a satisfactory result was obtained. For the remaining galaxies, we imposed as a photometric zero point to the HST profiles (F814W) the mean offset between the aperture magnitudes measured on the 2MASS and HST images in the radial range 7–12″, which depends on an estimate of the sky background level for the HST image; we then joined the HST and the calibrated ‘ground-based’ profiles, modifying our sky estimate for the HST image until a good match was obtained; given the fact that the field of view of WFPC2 is significantly larger than the one of NICMOS, this operation required much less careful fine-tuning than for the NICMOS profiles. At the end, calibrated global *H* – band profiles were obtained. We tested whether the use of WFPC2-F814W images in the cases where NICMOS is not available introduces significant additional errors: for several of the galaxies with available NICMOS imaging, we retrieved the F814W images and treated them in the way described above; the result is that the comparison between the final global profiles obtained this way and the ones obtained using NICMOS is acceptable, with differences below 0.1 mag outside the inner $\approx 1''.5$ and below 0.05 mag outside the inner $\approx 4''.5$. This means that we can be rather confident in using the F814W images for the inner regions, and that *I* – *H* colour gradients are not very important.

4 BULGE-DISK DECOMPOSITION

Fitting a parametric bulge and disk can be done directly on the 2-dimensional images, or on one-dimensional profiles, that have been obtained by averaging azimuthally in ellipses or circles. Although one-dimensional profiles suffer from loss of information due to projection, and produce larger degeneracies between bulge and disk parameters (de Jong (1996a)), two-dimensional fits are less robust, and degeneracies remain (Möllenhoff & Heidt 2001). On the basis of their simulations MacArthur et al. (2003) conclude that a full two-dimensional technique does not provide a significant improvement compared to one-dimensional methods in recovering the axisymmetric structural parameters. Based on this, we have chosen an approach that allows us not to have to assume the same shape of bulge and disk, but for which we do not have to apply a full two-dimensional fitting method, as we will explain in the following sections. Alternatively, we could have used a non-parametric fitting method, such as the method of Kent (1984), where two components are found with different axis ratios, but have not done this, because of the degeneracies that arise when choosing the axis ratios of these components.

4.1 Decomposing late-type spirals

We performed a non-simultaneous bulge-disk decomposition for our 18 galaxies, closely following the method described by Noordermeer (2006) and Noordermeer & van der Hulst (2006) and previously introduced by Palunas & Williams (2000). In a few words, we fit an exponential law to the disk, marking the fitting range via a visual inspection of the profiles, choosing the part of the profile that is exponential without doubt; we build a model image of the disk and subtract it from the original images, obtaining

‘bulge images’ from which we extract the ‘bulge profiles’ that we then fit with a Sérsic $r^{1/n}$ law.

4.1.1 disk fitting

The first step in our bulge-disk decomposition is the estimation of the disk parameters by means of profile fitting. On the combined global profiles, measured as explained in Section 3, using a least-square algorithm we fitted an exponential light distribution (in mag arcsec⁻²):

$$\mu_d(r) = \mu_{0,d} + 1.0857 \left(\frac{r}{h} \right) \quad (1)$$

where $\mu_{0,d}$ and h are the central surface brightness and scale length of the disk. The actual fit was performed on the profiles in absolute magnitudes and on radial ranges chosen by means of a visual inspection, in order to avoid the contamination from the central component (the ‘bulge’). The choice of a fitting range became a sort of ‘compromise’ in a few cases where the shape of the profile would have suggested the presence of a double disk (see Pohlen & Trujillo 2006). Fig. 1 shows the global galaxy profiles, together with the best-fitting exponentials, and the residuals from the fit. The radial ranges of the fits are indicated in the residual plot. These figures show that in general the fits are satisfying. NGC 4102 represents the case where the fit is worst; this might be due to contamination from the big bar, or from the coexistence of an inner and an outer disk (see also Pohlen & Trujillo 2006), to which we impose a single-exponential fit.

The fit parameters are listed in Table 2. No correction for inclination or galactic extinction is applied. The uncertainties of these parameters can be calculated in various ways. Often uncertainties in the least-squares fit are quoted. These are often very small, since galactic disks can be fitted very well with an exponential surface brightness profile, if a limited radial fitting range is used (de Vaucouleurs 1959, Freeman 1970, MacArthur et al. 2003, Pohlen & Trujillo 2006). By changing the radial range, however, disk parameters can vary considerably. Therefore, a more realistic estimate of the uncertainties in surface brightness and scale length is obtained if one studies the variation of these parameters as a result of changing the fitting range. To do this, we varied both the inner and outer radial limit by steps of 5%, from 70% to 130% of the range quoted in Table 2. The final parameters disk are the average parameters obtained in this way, and the uncertainty the RMS scatter.

4.1.2 Bulge fitting

In all cases, in the innermost regions the galaxy’s light clearly exceeds the exponential fit to the disk. According to the photometric definition (see the Introduction), the region of the galaxy corresponding to this light excess is the bulge. We will adopt this definition, but without implications on the kinematics and/or populations: without implying that it has to be a hot and old component, similar to a *small elliptical*.

To quantify the region where the light from the bulge is significant, we established a *bulge radial extension*, defining as *bulge* the region within which the intensity ratio between the fitted exponential disk and the total intensity is lower than 0.7 (i.e. the bulge contributes to 30 percent or more of the total light, see Fig. 1 and Table 2). Note that these figures can be affected by the presence of bars or other asymmetric features not belonging to the exponential disk.

On the basis of the fitted disk parameters, using the standard

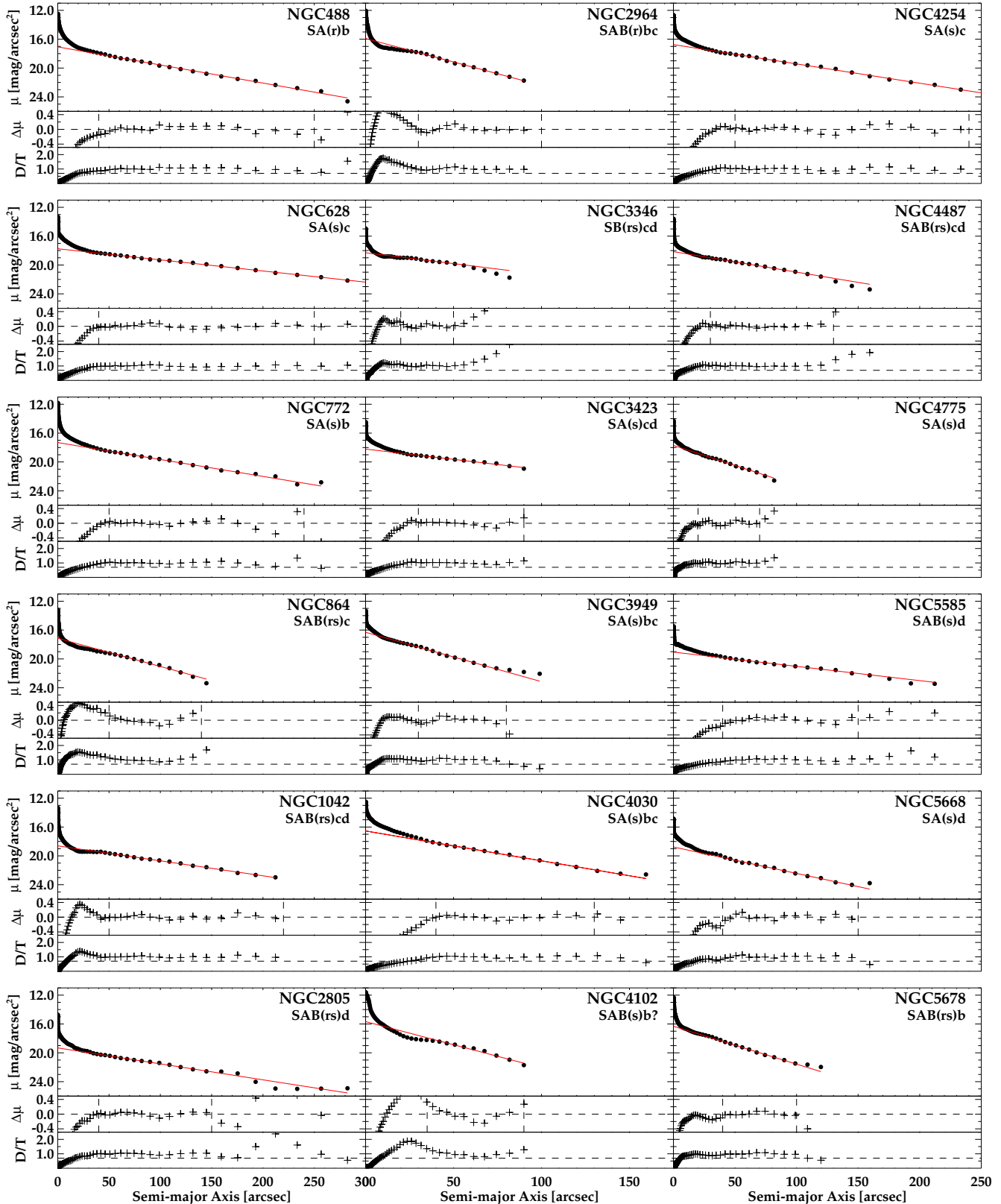


Figure 1. Global combined photometric profiles and exponential fits to the disks. Filled dots show the global combined photometric profiles, along with the best-fitting exponential (solid line). The units are arcsec along the semi-major axis of the ellipses on the horizontal axis and absolute H magnitudes arcsec⁻² along the vertical. Below each profile the residuals from the fit are shown, in the same units. Below the disk to total ratio of the fitted exponential disk and the total profile intensity is shown; the level $D/T = 0.7$ is indicated (dashed line), defining the ‘bulge region’, as explained in the text.

IRAF tasks (BMODEL in the STSDAS.ANALYSIS.ISOPHOTE package) we built a model image of the disk and subtracted it from the original 2MASS images. We will refer to the residual images as the 2MASS ‘bulge image’. From these images we extracted the bulge photometric profiles and parameters, by applying a procedure similar to the one used to measure the ‘total’ profiles as explained in Section 3: we fitted ellipses to the bulge images in two steps, keeping in all cases the centre fixed to the value already determined for the original 2MASS images and the position angle fixed to the value determined from the DSS images in Section 3. At first, we left the ellipticity free; in a second step we fixed also the ellipticity and extracted the intensity profiles from the 2MASS bulge images, successively converting them to an absolute magnitude scale, applying the offset given by the keyword MAGZP in the 2MASS headers. As ellipticity for the bulge we adopted a representative value estimated within the bulge region, on the basis of the ellipticity profiles extracted from the 2MASS and HST images. We notice that bulge and disk ellipticities can be different. Fig. 2 presents a comparison between the adopted values for the ellipticities of disks and bulges, showing that for most of the galaxies the inner component is rounder than the disk; but in some cases (NGC 3346, 4487, 4775, 5668, among the latest-type objects in our sample), the bulge is instead flatter than the disk, as shown also by Fathi & Peletier (2003) on the basis of the bulge-disk decomposition of 70 disk galaxies spanning a range in type between S0 and Sm. Only NGC 3346 lies more than 1σ above the 1:1 relation in Fig. 2.

Once the bulge and disk profiles have been retrieved, we need to determine the structural parameters by fitting a model profile. We follow the approach most often used in the current literature (see Graham & Worley 2008 for a comprehensive review) by fitting an exponential disk and a Sérsic $r^{1/n}$ bulge.

When fitting the profiles, seeing effects are particularly relevant when the effective radius is small and/or when the ratio between the effective radius and the FWHM of the seeing is small (Graham 2001). In fact, for small bulges poor seeing could smear the images so that bulges intrinsically described by $n > 1$ Sérsic profiles could appear like $n < 1$ profiles. Therefore, for a reliable treatment of the seeing effects, we performed the fit on the *bulge region* by convolving the Sérsic profiles with a Gaussian point-spread function, as explained by Graham (2001), and then fitting the seeing-convolved Sérsic profiles using a standard non-linear least-squares algorithm. The values of the FWHM of seeing in the 2MASS images were retrieved from the header keyword SEESH via the relation $\text{FWHM}(\prime) = 3.13 \times \text{SEESH} - 0.46$ as explained on the 2MASS webpage³. In some cases (e.g. NGC 864, 2964, 3346, 3949, 4775 and 5678) the bulge region is so small that it is comparable in size with the FWHM of seeing in the 2MASS images (less than $3 \times \text{FWHM}$ of the seeing), so that the applied procedure is not meaningful and possibly leads to imprecise fitting values. In order to face this problem, to gain spatial resolution in the inner parts, and to take advantage of data non contaminated by seeing effects, we perform the bulge fitting on bulge profiles extracted from the HST images (NICMOS or F814W, depending on availability). These profiles were obtained by subtracting from the HST images an exponential disk, modeled on the basis of the fit parameters obtained as described in Section 4.1.1, and then fitting to the residual images ellipses with position angle and ellipticity fixed to the ‘disk position angle’ and the ‘bulge ellipticity’, and centre coordinates fixed as well. Some of these ‘HST bulge profiles’ suffer

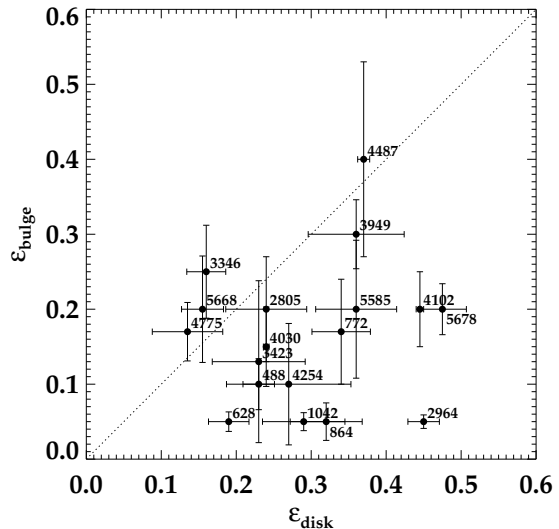


Figure 2. Bulge against disk ellipticities; each filled dot represents a galaxy, with the NGC number indicated close to the symbol. The disk ellipticity is determined from the outer parts of the galaxies, the bulge ellipticity from the inner regions, as explained in the text. The dotted line represents the 1:1 relation. The overplotted error bars are obtained from the scatter of the points in the profiles.

from the complementary problem of limited spatial extension: in several cases they do not cover the full bulge region. In those cases (NGC 488, 628, 772, 4030, 4254, 4775, 5668) we joined them with the bulge profiles previously obtained from the 2MASS images. On these profiles we fitted a pure Sérsic law, excluding the very innermost parts ($0.5-1''$), which in several cases host nuclear star clusters. In Fig. 3 we show the HST or joined HST + 2MASS bulge profiles, along with the best-fitting Sérsic profile, and the residuals from the fit.

The fit parameters for all galaxies, for both the disk and the bulge components, are listed in Table 2. Here we report the disk parameters from the exponential fit as in Section 4.1.1; for the bulge we quote the parameters from the seeing-convolved Sérsic fit to the 2MASS bulge profiles and those from the Sérsic fit to the HST or combined 2MASS-HST bulge profiles. No correction for inclination or galactic extinction is applied to the surface brightness (and magnitudes) values reported in the table. The uncertainties of the bulge parameters have been calculated in the same way as for the disk, i.e. by varying the fitting range by 30% for both the inner and outer boundary. Fig. 4 shows the comparison between the two sets of parameters for the bulge; the effective surface brightness and radius are generally rather similar, while the Sérsic parameter n tends to be larger for the fits on the HST (or combined HST + 2MASS) profiles. In the following, for the bulge parameters we will refer to the output of the fit on these latter profiles. From the parameters we computed the total bulge and disk luminosities (see Graham 2001), and converted them to absolute magnitudes M_d and M_b using the distance moduli used by Ganda et al. (2006). These numbers, together with the bulge to disk ratio, are also given in Table 2.

³ www.sao.arizona.edu/FLWO/2mass/seesum.html

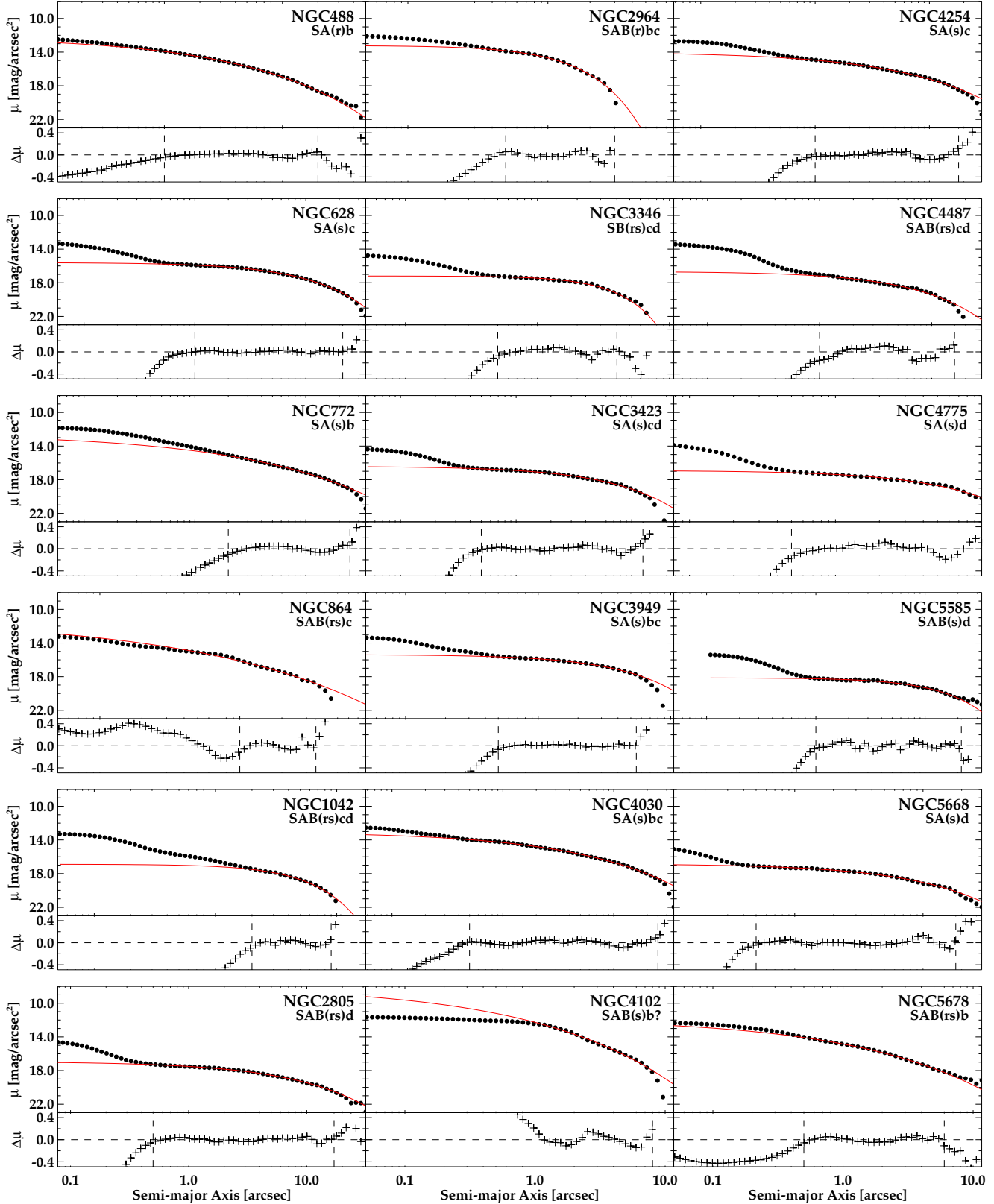


Figure 3. Sérsic fits to the bulge profiles. In the top part of each panel we plot the HST or combined HST + 2MASS bulge profiles (filled dots), in mag arcsec⁻²; the NICMOS images are used in all available cases, the F814W-WFPC2 in the others (see Table 1); overplotted are the best-fitting Sérsic profiles (solid line); The low part of each panel shows the residuals from the fit (in mag arcsec⁻²), as well as the fitting range (vertical lines). Note that the abscis is given in logarithmic units, contrary to Fig. 1.

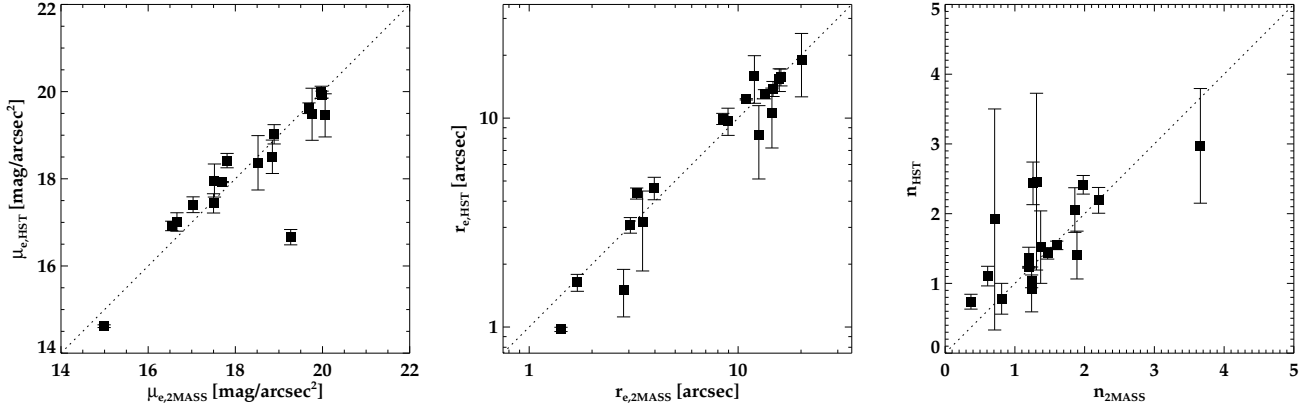


Figure 4. Comparison between the fitted parameters for a seeing-convolved Sérsic fit performed on the 2MASS bulge profiles and a pure-Sérsic fit on the HST or joined HST + 2MASS bulge profiles, excluding the innermost region: from left to right, effective surface brightness, effective radius, n . The dotted line in each panel represents the 1:1 relation.

NGC	$r_{d,i}$	$r_{d,o}$	$\mu_{0,d}$	\pm	h	\pm	$r_{bu,i}$	$r_{bu,o}$	$\mu_{e,2m}$	$r_{e,2m}$	n_{2m}	$\mu_{e,hst}$	\pm	$r_{e,hst}$	\pm	n_{hst}	\pm	M_d	M_{bul}	\pm
(1)	(2)	(3)	(4)	(5)	(6)	(7)	(8)	(9)	(10)	(11)	(12)	(13)	(14)	(15)	(16)	(17)	(18)	(19)	(20)	(21)
488	40	250	17.03	0.07	42.7	1.1	1	20	16.54	8.5	1.98	16.92	0.11	9.9	0.6	2.41	0.13	-25.70	-23.77	0.05
628	40	250	17.75	0.03	70.7	1.1	1	21.5	17.70	10.9	1.20	17.92	0.01	12.3	0.1	1.23	0.01	-23.50	-20.31	0.01
772	50	240	17.35	0.06	47.1	1.2	2	25	18.52	20.1	3.66	18.37	0.62	19.0	6.4	2.9	0.8	-25.82	-24.07	0.25
864	50	140	17.13	0.30	28.1	2.7	1	4	16.66	1.7	0.71	17.01	0.21	1.6	0.2	1.9	1.6	-23.85	-18.78	0.42
1042	50	220	18.62	0.02	52.5	0.7	2	9	17.81	3.3	1.24	18.42	0.16	4.4	0.3	0.91	0.32	-23.32	-18.75	0.14
2805	40	150	19.36	0.06	50.8	1.8	0.5	17	19.99	13.4	1.60	19.93	0.08	13.0	0.7	1.55	0.06	-23.46	-20.84	0.05
2964	30	100	15.96	0.07	16.9	0.3	0.5	3	14.99	1.4	0.37	14.62	0.03	1.0	0.0	0.74	0.11	-23.79	-19.47	0.04
3346	20	50	18.28	0.14	35.4	4.5	0.5	4	18.85	3.5	0.81	18.51	0.38	3.2	1.3	0.78	0.22	-22.90	-17.99	0.35
3423	30	90	18.28	0.08	40.1	2.5	0.5	12.5	18.89	8.9	1.20	19.02	0.22	9.7	1.4	1.37	0.15	-22.63	-19.64	0.15
3949	30	80	16.48	0.29	16.8	1.6	0.5	5.5	17.03	4.0	0.61	17.41	0.18	4.6	0.6	1.10	0.14	-22.51	-19.52	0.13
4030	40	130	16.55	0.09	26.5	0.8	0.5	25	17.50	15.7	2.20	17.44	0.22	15.3	1.9	2.19	0.18	-24.22	-23.23	0.10
4102	35	90	16.03	0.45	19.5	3.1	1	8.5	14.12	2.8	1.31	12.99	0.62	1.5	0.4	2.5	1.3	-23.40	-22.00	0.25
4254	50	240	16.76	0.04	40.7	0.6	1	18	17.52	12.0	1.86	17.96	0.38	15.8	4.1	2.05	0.32	-24.78	-22.57	0.20
4487	30	130	18.07	0.12	36.8	2.4	1	10	19.76	14.5	1.37	19.48	0.60	10.6	3.4	1.52	0.52	-22.64	-19.41	0.30
4775	20	70	17.67	0.06	19.3	0.6	0.5	6.5	20.06	12.6	1.89	19.46	0.49	8.3	3.2	1.41	0.34	-22.55	-19.79	0.37
5585	40	150	19.00	0.09	53.2	2.9	1	21.5	19.97	16.0	1.24	19.98	0.14	15.7	1.5	1.03	0.09	-21.26	-18.33	0.10
5668	40	150	18.80	0.16	30.3	1.7	0.5	18	19.69	14.7	1.47	19.62	0.12	13.8	1.1	1.43	0.08	-22.54	-20.89	0.09
5678	40	100	16.34	0.25	20.9	1.7	0.5	6	19.27	3.1	1.26	16.66	0.18	3.1	0.3	2.43	0.31	-24.78	-21.42	0.08

Table 2. Column (1): NGC identifier; columns (2) and (3): disk fitting range, in arcsec; columns (4) and (6): respectively, central surface brightness of the disk in mag arcsec $^{-2}$ and scale length of the disk in arcsec, from the fits performed on the photometric profiles in Section 4.1.1; column (5) and (7) indicate their uncertainties; columns (8) and (9): bulge fitting range, in arcsec; columns (10), (11) and (12): effective surface brightness in mag arcsec $^{-2}$, effective radius in arcsec and Sérsic parameter (n) of the bulge from the fit of a seeing-convolved Sérsic profile to the bulge profiles extracted from the 2MASS images; columns (13), (15) and (17): bulge parameters (effective surface brightness, effective radius and Sérsic parameter (n)) from the fit of a Sérsic profile to the HST or joined HST + 2MASS bulge profiles, with uncertainties in columns (14), (16) and (18); columns (19) and (20): H – band absolute magnitudes of the disk and bulge components, and the uncertainty in the latter (21). The uncertainties quoted here are the variations due to changing the fitting ranges.

5 OPTICAL PHOTOMETRY AND OPTICAL – NIR COLOURS

As we mentioned in the Introduction and as we witnessed throughout this work, late-type galaxies are known to be dusty objects, with dust lanes and structures extending often all the way to the centre (Frogel 1985, Zaritsky, Rix & Rieke 1993, Martini et al. 2003). For example we just mentioned in the previous section that dust makes it sometimes difficult to investigate the properties of tiny inner components. This is one of the reasons for which we decided to work in the near-infrared. In order to investigate the amount and distribution of extinction in the centers of these objects, we decided to

analyse also optical images. Here, the fact that we have absorption line strength maps determined with SAURON offers a large advantage, when compared to previous work. Comparing optical-near infrared colours, affected by extinction, with absorption line index maps, which are almost not affected, we can obtain a reasonably accurate guess of the amount of extinction in the central regions of a representative sample of late type spirals. There are 13 galaxies for which F606W HST images are available in the HST archive. For 10 of them, also NICMOS F160W images are available. We decided to analyse these 10 galaxies.

5.1 Optical – Near-infrared colour profiles

We analyzed the optical images in the same way as the NIR ones, with the exception that here we used the POSS-II Red IIIaF + RG610 images in the outer parts: using the IRAF task ELLIPSE we first extracted from the DSS images photometric profiles with centres and geometric parameters free and determined the centres coordinates; we then fixed the centres and extracted again profiles with free ellipticities and position angles. In many cases in the outer parts the geometric parameters converge to a constant value; in the majority of cases this value is comparable with what found in the NIR: we did not detect any significant difference in the shape of isophotes between optical and near-infrared. Therefore, we fixed the position angle and ellipticity to the values determined on the NIR images (see Table 1) and measured the intensities along the ellipses. We then subtracted the sky background, estimated by averaging the mean values of intensity in several boxes placed in the outer parts of the images, and converted the profiles to a (uncalibrated) magnitude scale. For the HST F606W images, we started by creating mosaic images of the four chips, using the IRAF task WMO-SAIC, rotated them to bring them to the standard orientation with North up-East left and extracted from them intensity profiles with centre, position angle and ellipticity fixed (fixed to the NIR values); we then subtracted an estimate for the sky background and converted the profiles to a (still uncalibrated) magnitude scale. Then we combined HST and DSS profiles into single profiles, aligning them at the level of the HST profiles; when a good matching of the two was not achieved, we modified the estimated sky brightness in the HST image, until the matching was satisfactory. The last step is the photometric calibration: converting the profiles to an absolute magnitude scale. We calibrated our profiles to the $V - I$ band of the UBVRI Johnson-Cousin system using the equations provided by Holtzman (1995), that were derived for single-chip images. To be able to apply those transformations, for each galaxy we focused on the single-chip image containing the galaxy centre (PC1 for all galaxies excluding NGC 1042 and 3949, centred instead on WF3) and extracted the single-chip profiles. The sky subtraction is in this case more difficult, since the field of view is significantly smaller: we proceeded in an iterative way, changing the estimated value of the sky background until the sky-subtracted single-chip profile matched the shape of the sky-subtracted profile retrieved from the mosaic image. We then calibrated the single-chip profiles applying Equation 9 in Holtzman (1995), using the coefficients listed in his Table 10:

$$\begin{aligned} \mu_V = & -2.5 \times \log(\text{counts}) + 2.5 \times \log(\text{EXPTIME}) + \\ & + 5 \times \log(\text{SCALE}) + 0.254 \times (V - I) + 0.012 \times (2) \\ & \times (V - I)^2 + 22.093 + 2.5 \times \log(\text{GR}) + 0.1 \end{aligned}$$

where ‘counts’ is the number of counts in linear units, ‘EXPTIME’ the integration time on the image, ‘SCALE’ the pixel scale (arcsec pixel⁻¹, ≈ 0.046 for the galaxies centred on PC1 and ≈ 0.09944 for the two centred on WF3), $V - I$ the colour in the Johnson-Cousins UBVRI system, 22.093 the photometric zero point tabulated by Holtzman (1995), GR equals 2.003 for frames where a gain of 14 was used, and 1 otherwise, and 0.1 is added, following the prescription of Holtzman (1995), in order to correct for infinite aperture (see also the WFPC2 Data Handbook). For the $(V - I)$ colours of our galaxies we used values from HyperLeda and, when not available, an average of the values for galaxies of the same Hubble type. Since the colour term is relatively small, there is no need for extremely accurate

NGC	$V - I$	NGC	$V - I$
488	1.16	3949	0.81
628	1.38	4030	1.20
864	1.28	4102	1.23
2964	1.28	5585	0.88
3949	0.81	5678	1.19

Table 3. Values for the colour $V - I$ adopted in the calibration of the optical images from HST.

values here. The adopted values are listed in Table 4. The last step was to find and apply the vertical offset necessary to align the HST(mosaic) + DSS joined profiles to the calibrated single-chip profiles.

Four of the galaxies for which we perform our optical analysis (NGC 1042, 3423, 4030 and 4102) belong also to the sample studied by Pohlen & Trujillo (2006), who present SDSS g' and r' profiles (roughly corresponding to B and R bands) for 90 almost face-on late-type galaxies. The authors kindly provided us their profiles for the galaxies in common. In their profiles we recognize all the features that we see in ours, at the same radii, out to $\approx 150 - 200''$ (depending on the galaxy): the profiles are completely consistent, with the caveat that they are measured in different bands.

From the thus obtained V and H profiles we determined radial $V - H$ colour profiles, that we present in Fig. 6. Here we only present the inner $20''$, since real near-infrared imaging is only available in this region. Further out, the 2MASS images are not deep enough. We find that the profiles have large dispersions in colour, and a wide variety in slope. Some galaxies become redder, some bluer as a function of radius. When comparing them to elliptical galaxies (e.g. Peletier, Valentijn & Jameson 1990) the profiles are much less smooth, and the gradients much larger. The colour maps are very instructive in telling us what is happening. Fig. 7a and 7b show the calibrated $V - H$ colour maps of the inner $20'' \times 20''$ of the galaxies. They have been displayed on the same scale, to make it easier to make the comparison from galaxy to galaxy, and to compare the internal gradients with the colour differences from galaxy to galaxy. The colour maps show dust lanes in all galaxies except for NGC 5585, spiral arms with younger stars, inner spirals, nuclear clusters, etc. In most cases it is not easy to find out where the galaxy center is, when just looking at the colour map.

5.2 Extinction in the centers of late-type spiral galaxies

From a $V - H$ map alone it is very difficult to determine the amount of extinction E_{V-H} . The problem is that the intrinsic colour of the stars is unknown, so that the uncertainty in the colour of the stars is reflected in the uncertainty in the amount of extinction. Having two colours does not help very much, since the effects of reddening in colour-colour diagrams is almost parallel to the effect due to changing metallicity or age (e.g. Kuchinski et al. 1998), and since the distribution of the dust changes the relative extinction in the different bands. Determining the amount of extinction in a specific galaxy is therefore done assuming a certain colour for the stellar populations (see e.g. Knapen et al. 1995), using the Balmer decrement for ionised gas (which usually gives the extinction on the line of sight to an HII region, but not in the whole galaxy), or using statistical methods. For example, from the distribution of colour

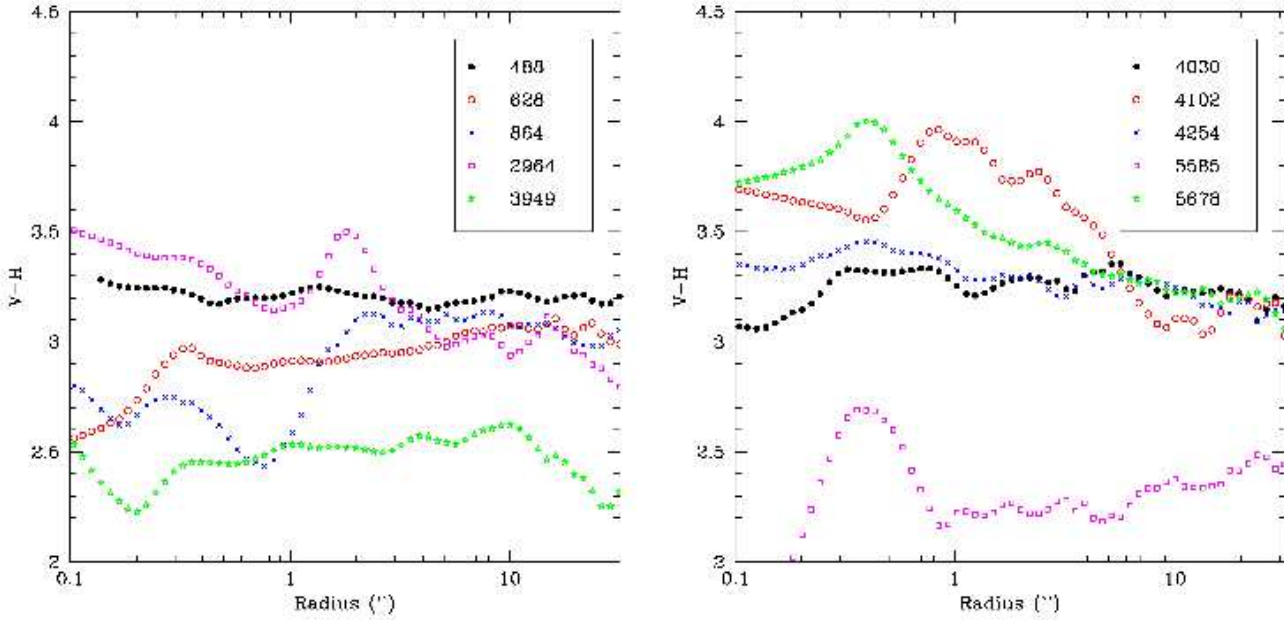


Figure 5. $V - H$ colour profiles for the 10 galaxies with available optical and NIR HST images

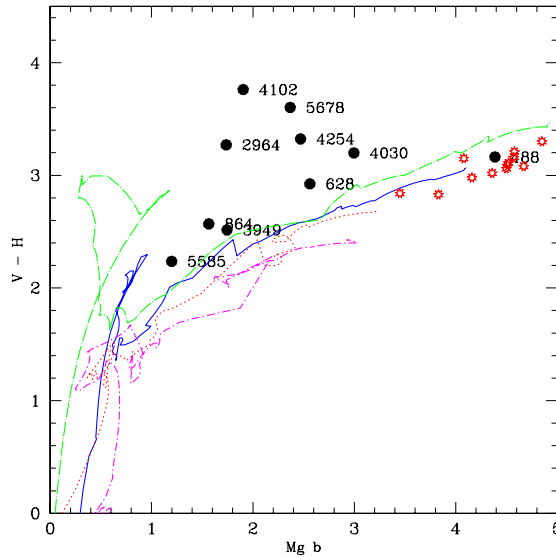


Figure 6. $V - H$ colour vs. $Mg\ b$ line strength in central apertures of $2.4''$ for the 10 galaxies with NICMOS F160W and F606W HST data (black filled symbols). In red (asterisks) elliptical and S0 galaxies are shown from Kuntschner et al. (2006), with $V - K$ measurements from Frogel et al. (1978). Lines represent SSP models of Bruzual & Charlot (2003) for various metallicities: green (long dashed-dotted) indicates $Z=0.05$, blue, full lines indicate $Z=0.02$, red dotted line $Z=0.008$ and magenta short-dashed-dotted lines $Z=0.004$.

as a function of inclination one can derive the amount of extinction (e.g. Tully et al. 1998, Giovanelli et al. 1995, Peletier et al. 1995). The SAURON dataset offers the nice advantage that absorption line indices are available in the inner $40'' \times 30''$. Since to first order the $Mg\ b$ index in a galaxy gives the same information as the $V - H$ colour (which is the metallicity for an old galaxy, see Fig. 6), and since $Mg\ b$ is affected very little by extinction (MacArthur 2005), one can use the $V - H$ and $Mg\ b$ together to determine the amount of extinction at every position where both are avail-

able. Here we use the central $Mg\ b$ measurements of Ganda et al. (2007) to calculate the extinction in the central aperture with diameter $2.4''$. In Fig. 6 these central values are shown. The figure shows that the models with various metallicities almost fall on top of each other. This means that one can measure the extinction by measuring the distance in $V - H$ to a line of models with a given reference metallicity. Since most of the galaxies have luminosities similar to the Milky Way, we take the solar models as a reference. For NGC 5585, which is fainter, it is probably more appropriate to

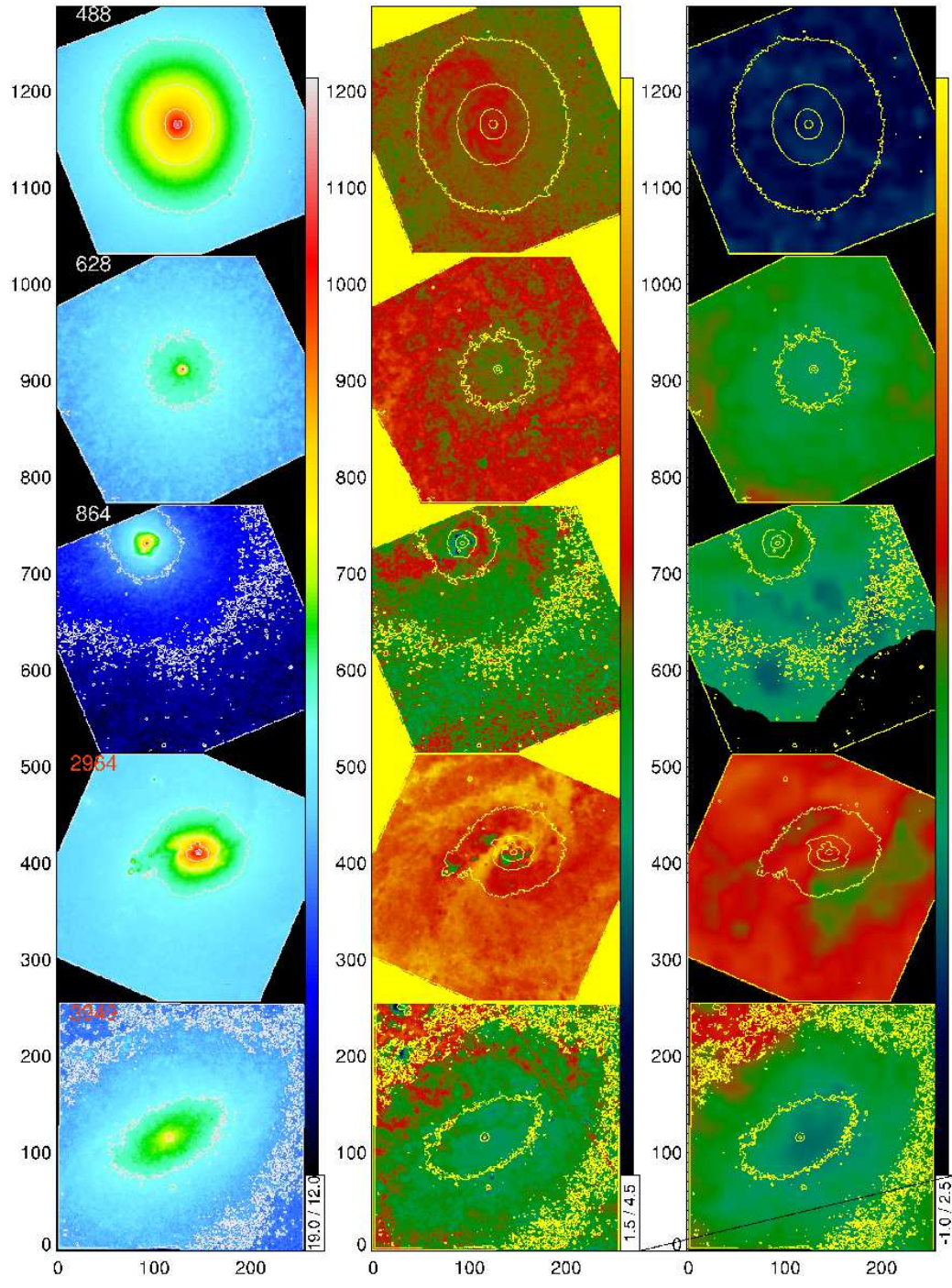


Figure 7. (a): Extinction distribution for the 10 galaxies with space-based photometry in F606W and F160W. Left: surface brightness distribution in H. Middle: calibrated V-H colour maps. Right: extinction maps from $V - H$ and $Mg\ b$. The ranges of the plots are shown in the lower right of each column of plots.

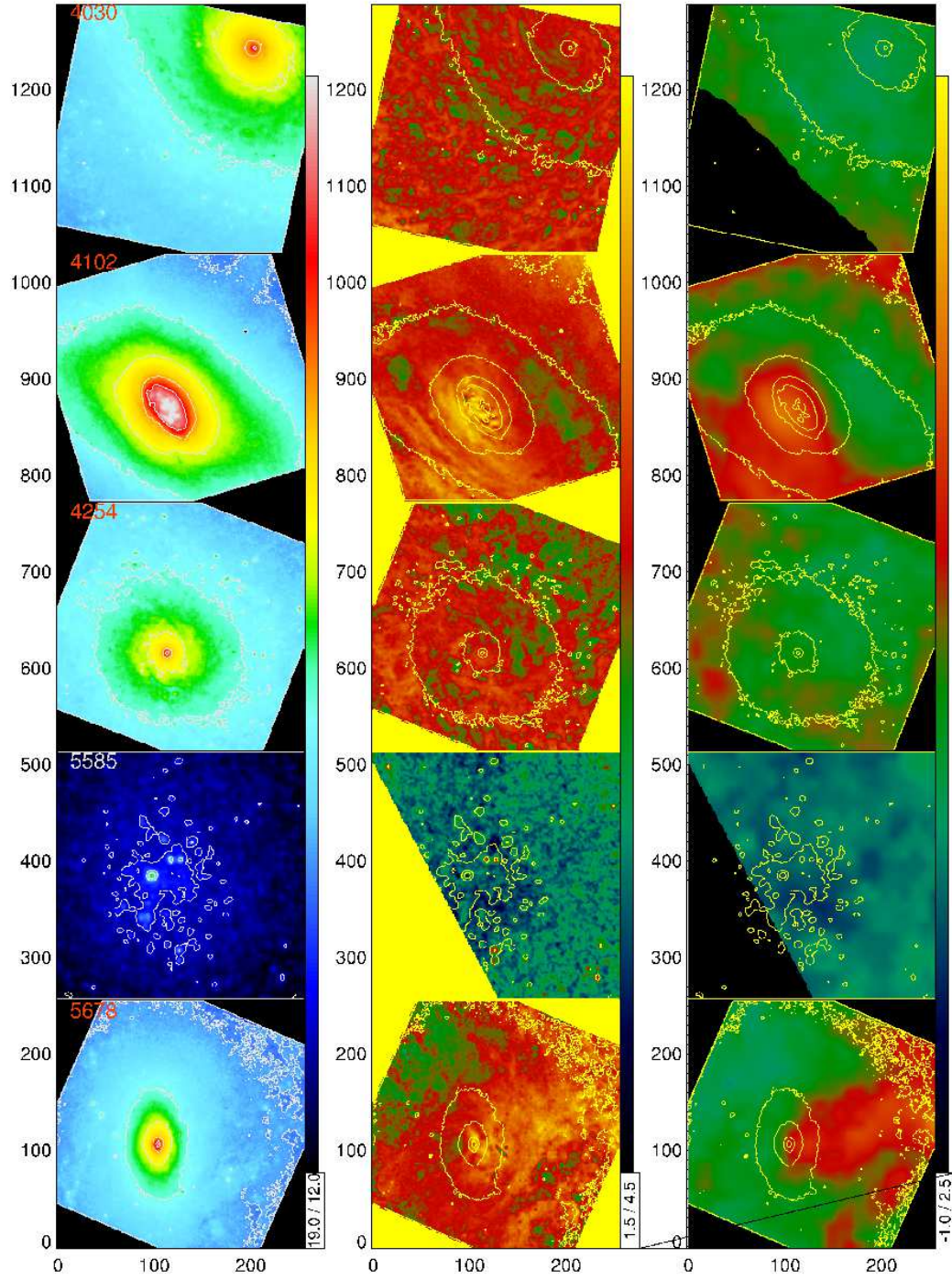


Figure 7. (b): Extinction distribution for the 10 galaxies with space-based photometry in F606W and F160W. Left: surface brightness distribution in H. Middle: calibrated V-H colour maps. Right: extinction maps from $V - H$ and Mg b.

NGC	$V - H$	E_{V-H}	A_V	NGC	$V - H$	E_{V-H}	A_V
488	3.16	0.00	0.00	4030	3.20	0.47	0.57
628	2.92	0.33	0.40	4102	3.76	1.44	1.75
864	2.57	0.35	0.42	4254	3.32	0.74	0.90
2964	3.27	0.90	1.09	5585	2.24	0.22	0.27
3949	2.52	0.14	0.17	5678	3.60	1.05	1.27

Table 4. $V - H$ and central extinction in an aperture of diameter $2.4''$ derived from $V - H$ and Mg b (see Fig. 6).

take a lower metallicity. The uncertainty in the amount of extinction is then given by the uncertainty in the $V - H$ of the stellar populations in the galaxy that make up the Mg b. From the dispersion between the SSP models we estimate that this uncertainty is about 0.2 mag or less, even if the stellar populations consist of a mix of ages, since more complicated models are always linear combinations of SSPs. The obtained E_{V-H} values are converted to A_V using the Galactic extinction law (Rieke & Lebofsky 1985), dividing them by 0.825. Here the assumption is made that the galaxies are not optically thick in H . Given the extinction values that are obtained, this assumption is easily satisfied. Table 4 shows the extinction values we derived. We find an average E_{V-H} of 0.56 mag, or a lower limit to the average extinction $A_V=0.68$ mag. In Fig. 7 the central extinction maps, determined in this way, at the SAURON resolution, are shown.

Do we learn anything about the stellar populations from the $V - H$ colour? Figure 6 shows that we don't. For some galaxies $V - H$ is redder than for the most massive giant ellipticals. Since the line indices of all objects are weaker than those of massive giant ellipticals, we have a strong indication that it is dust extinction, and not large numbers of very red stars, that causes the red $V - H$ colour. This argument is made stronger by the fact that for highly inclined galaxies optical-infrared colours in regions outside the dustlane always are bluer than those of giant ellipticals (Peletier & de Grijs 1998). The issue of the very red optical-infrared colours was already discussed in 1985 by Frogel, who found galaxies with $V - K$ colours that were considerably redder than those of the brightest giant ellipticals. He found also that half of his sample of Sc galaxies had $U - V$ colours that were bluer than the giant ellipticals. Although he could not uniquely determine the extinction, he used the following experiment. If all galaxies had an intrinsic stellar population colour of $J - H=0.65$, he obtained extinction values between 0 and 1.64 mag in A_V . The optical-infrared colours would not be redder any more than those of giant ellipticals, and also reasonable $U - V$ colours would be obtained. Independently, Turnrose (1976) had derived internal extinction by comparing simple stellar population models with observed optical stellar energy distributions, and had found similar extinction values. We have one galaxy in common with Frogel (1985), NGC 628, for which $V - H$ agrees within 0.1 mag.

Since these are all close to face-on galaxies, the measured extinctions are not very different from what one would see if they were face-on. The extinction correction to face-on is given by,

$$\Delta\mu_V = \gamma \log(a/b)$$

where a/b is the axis ratio of the galaxy, and γ a transparency index (Boselli & Gavazzi 1994). For this sample $\log(a/b)$ ranges from 0 to 0.26, while values for γ should be between 0.4 and 0.7 (Boselli & Gavazzi 1994), so that the face-on corrected A_V is between 0 and 0.2 mag less than the value given in Table 4, sometimes still around or above 1 mag. This result is compatible with Tully et al. (1998),

Peletier et al. (1995) and Giovanelli et al. (1995), who used a statistical method, deriving the extinction from the relation of colour, or surface brightness, as a function of inclination.

We now look at extinction as a function of morphological type. This is shown in Fig. 8. The relation is not very clear, but it can be understood when one looks at the outliers. The galaxy of morphological type 7 (Sd, NGC 5585) is by far the bluest, and the smallest and has little extinction. This is in agreement with Tully et al. (1998) who find that galaxies with $M_B=-18$ have almost no extinction. At the other end, at morphological type 3=Sb, we find a galaxy with very little extinction, NGC 488, and two others with a lot of extinction. This can be understood by looking at Fig. 12 of Terndrup et al. (1994), where one can see that galaxies with type 3-5 have much more extinction than galaxies of earlier types. Peletier & Balcells (1996) confirm this, showing also that the extinction in galaxies of type 7 and larger is again much smaller than in galaxies of type 3-6. It looks as if NGC 488 is more similar to an Sab galaxy than an Sb in its inner regions. One should note that the A_V values that we have derived here are still lower limits. For example, by adding very young stellar populations mixed with dust, one can still make the color of a galaxy bluer. For that reason, the conclusion that the center of NGC 3949 is almost dust free is most likely wrong looking at the structure in the colour map. Our derived extinction values for these late-type spirals are consistent with Tuffs et al. (2004), who use the models of Popescu et al. (2000) to determine the attenuation of dust in spirals using a thin and a normal disk with extinction, and a bulge without dust. We should note that this models has a very large optical depth ($\tau_{B,cen} = 3.8$) so that, according to the model, we basically only see the bulge light in front of the disk, as a result of which the integrated reddening is not so high, and the colours reasonable. With these data we are not able to verify whether this extinction model is realistic for late-type spirals.

Does the finding that many of our late-type galaxies have a considerable amount of extinction in their centre have other consequences? Martini et al. (2003), and Carollo et al. (2002) also show optical-infrared maps of similar galaxies, some of which are in common with us. They however do not show any calibrated color maps. To test the effects of extinction on the structural parameters, we also calculated the same parameters as presented in Section 5 in the V -band. In general, the differences were small, something which could have been expected from the fact that for these galaxies the colour profiles are generally reasonably flat. Since there are many galaxies with large colour gradients (see e.g. Martini et al. 2003 and Carollo et al. 2002) we think it is preferable to determine these parameters in the NIR only.

Peletier & Balcells (1996) show that colours of bulges and disks of spirals, measured in relatively dust free regions, are very similar, implying that stellar populations in bulges and inner disks are similar. Terndrup et al. (1994) find the same effect, but with more scatter in the colours, and with a sample that includes redder galaxies. As we do here, they claim that these galaxies are red because of internal extinction. The fact that bulge and disk colours, even for these red galaxies, are similar shows that similar amounts of extinction are present in both components. If galaxies are seen close to face-on, i.e. when most of the light comes from regions close to the symmetry plane of the galaxy, the colors of bulge and inner disk region both are affected by similar amounts of extinction. Images of edge-on galaxies show that the extinction is mainly situated in the plane.

Carollo et al. (2001) present a study of $V - H$ colours in a sample of bulges, also from HST imaging. To convert from her

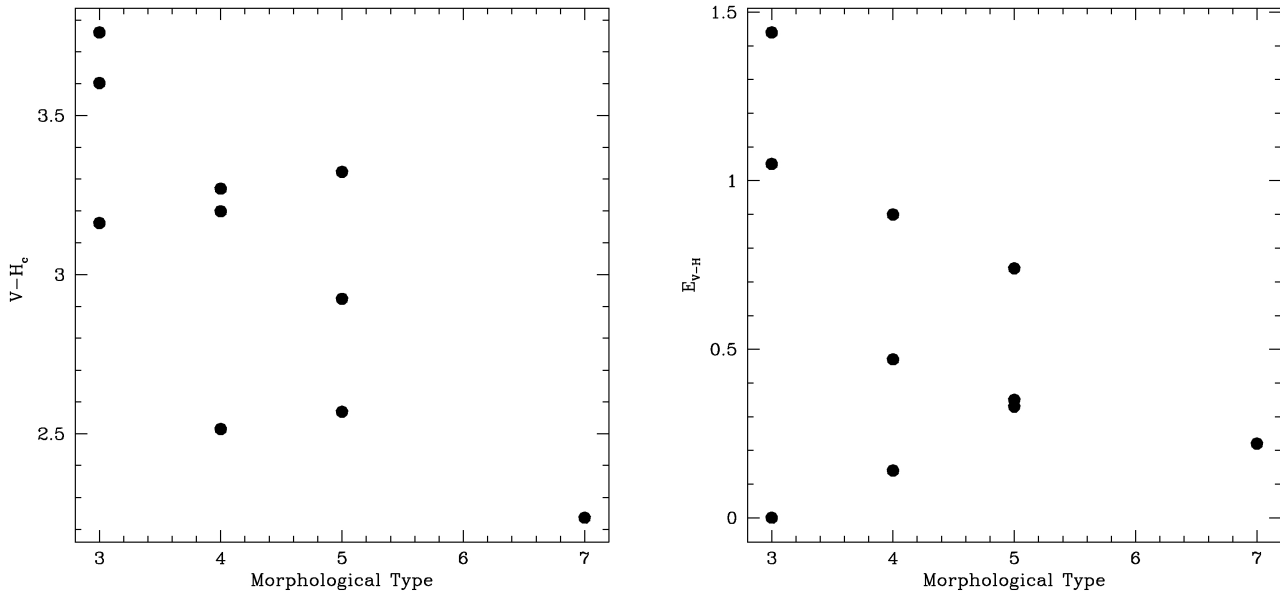


Figure 8. Left: Central V-H colour as a function of morphological type. Right: Central extinction E_{V-H} as a function of morphological type.

$V - H_{AB}$ colours to the Johnson system we use here we need to add 1.45 mag. By masking out patches of dust and star formation regions, they obtain $V - H$ colours that are blue enough that they can be explained by stellar population models, for both types of bulges discussed. However, the nuclei have often much redder colours, see their Fig. 3, that need considerable extinction. The problem with selecting *clean* regions by hand is that this method is subjective and probably not reproducible, giving results that are biased towards blue colours. The same is done in Carollo et al. (2007), where only one galaxy is found with optical-infrared colours redder than those of ellipticals and early-type bulges.

Dust can have important consequences for the interpretation of mass profiles from rotation curves and optical photometry. Without correcting for extinction, which is often impossible, the resulting stellar M/L ratios will be too large, and show a much larger scatter than is due purely by stellar populations. Since the dust extinction is largest in the central regions, and HI observations often have a limited angular resolution, the effect is most important when interpreting optical rotation curves. Palunas & Williams (2000) find that if they correct the surface brightness by $A_{I,int} = 1.0 \log(\frac{a}{b})$ the resulting M/L ratios do not vary any more as a function of inclination. In the V-band the correction should be larger by a factor ~ 1.5 . Such corrections in general are not very meaningful, since extinction varies as a function of radius. If one wants to obtain accurate M/L ratios in the centers of galaxies, one either has to work in the NIR only, or make detailed extinction corrections.

6 BULGE AND DISK PARAMETERS

Here we study the structural parameters determined in the previous Section together with data from the literature.

We quantitatively investigate the structural parameters obtained from the bulge-disk decomposition as a function of various fundamental galaxy parameters, such as morphological type, central velocity dispersion, and luminosity, to obtain a better under-

standing of the formation of these galaxies. Only the most noteworthy relations are shown here; additional relations, including those between disk and bulge parameters, are shown in Appendix B.

We concentrate, in particular, on how late-type spiral galaxies differ from earlier types. We do this by comparing our galaxies with the large literature compilation of Graham & Worley (2008), and with the recent sample of Fisher & Drory (2008). Graham & Worley present a compilation of about 10 samples, mostly in the near-infrared. Fisher & Drory analyse a sample of HST data, mostly in the optical. For the relations with central velocity dispersion we compare with the sample of early-type galaxies of Balcells et al. (2007b), hereinafter B07. For the literature samples, we took the numerical values from the tables available in the published papers, adjusting the scale lengths and effective radii in order to homogenise the adopted value for the Hubble constant to $H_0 = 70 \text{ km s}^{-1} \text{ Mpc}^{-1}$ (for consistency with what done by Ganda et al. 2006 and with the luminosities calculated in Section 4). The total magnitudes (of bulge and disk) of Balcells et al. (2007b) were converted from K to H using the typical colour for disk galaxies $H - K = 0.21 \text{ mag}$ (Frogel et al. 1978). For most of the relations that we will investigate and show graphically, we list in Table 5 the linear Pearson correlation coefficient c , calculated for the galaxies of our sample only. For the strongest correlations, with $|c| \geq 0.5$, we performed an outliers-resistant linear fit, assuming a dependence of the form $y = a + b \times x$, y and x being the variables involved and a and b the fit parameters. Those fits, for which the parameters are given in Table 6, are discussed in detail below.

6.1 Trends among the structural parameters

In Fig. 9 we show a number of structural parameter as a function of stellar velocity dispersion. Here one should note that due to the paucity of velocity dispersions in the literature we can only compare 2 samples of about 20 galaxies, of resp. early and late type spirals. There are some interesting things to note. Several papers, e.g. B07, Fisher & Drory (2008) and Graham & Worley (2008),

show that the Sérsic index n correlates reasonably well with bulge luminosity, with galaxy type and bulge to disk ratio, but with considerable scatter. Fig. 9a shows that the same holds for the central velocity dispersion σ . There are late-type spirals with velocity dispersions larger than 100 km/s, that show n -values considerably larger than 1. If all bulges of late-type spiral galaxies would be disks (also called pseudo-bulges), their n -values would be close to 1. This is however not the case, and it appears that the central velocity dispersion of the galaxy is determining the shape of the surface brightness profile of the bulge, rather than the galaxy type, which is determined more by the total star formation or the bulge to disk ratio. Consistent with this picture is the relation between bulge luminosity and central velocity dispersion. Already B07 found a tight relation between these 2 quantities for early-type spiral galaxies. Here we see that late-type spirals follow the same relation. So, even though the surface brightness of bulges of late-type spirals is lower than of early-type spirals, and the B/D ratio for a given velocity dispersion is lower as well (Fig. 9bc), the bulge luminosity - σ relation is the same for both samples of galaxies. Since there is a strong correlation between the bulge luminosity, or central surface brightness, or Sérsic index n (Graham & Driver 2007), and black hole mass, a relation which also holds for the luminosity and black hole mass of elliptical galaxies and S0's, it is tempting to assume that bulges of late-type spirals also lie on this relation, and that the formation of those bulges is closely linked to the black holes in late-type spirals. If a central black hole is associated with every bulge, it would also explain why the tight black hole mass vs. central velocity dispersion relation (Ferrarese & Merritt 2000, Gebhardt et al. 2000) can be reproduced with bulge luminosity replacing central velocity dispersion, but not with disk or total galaxy luminosity. The lack of correlation between the sizes of bulges and disk with central velocity dispersion for late type spirals might also be a result of the fact that bulges of late-type spirals are less concentrated objects with $n \sim 1$, which do not follow the homology of elliptical galaxies and elliptical-like bulges.

We also like to point out that it appears that bulges of early and late-type galaxies show systematic differences: on the average early type spirals with low central velocity dispersion have much more concentrated bulges and disks: not only are disks and bulges smaller, but also the surface brightness of both components is higher.

6.2 Trends with Stellar Populations

This sample is unique in the sense that its central stellar populations have been studied using stellar absorption lines, which are almost independent of extinction, by Ganda et al. (2007), so that we can investigate whether the stellar populations depend on the structural parameters discussed above. In other words, are the age and star formation history of a galaxy related to the way it is built, and viceversa? We try to address this issue by plotting the results of our bulge-disk decomposition against population parameters. A few noteworthy relations are discussed here. The rest of the relations are discussed in Appendix B.

Fig. 10 shows the Sérsic parameter n and the disk central surface brightness and as a function of the central $H\beta$ absorption, a measure of the age of the galaxy, and the star formation time-scale τ . The stellar population parameters refer to a central aperture of radius $1''.5$. One sees that n increases of decreasing $H\beta$. This implies that for objects with relatively young stellar populations, bulges are exponential, and that old bulges are more similar to objects with a de Vaucouleurs distribution. This would be the case if the ob-

jects in which recently stars have formed are all disk-like, i.e. pseudo-bulges, and that old bulges are more spheroidal-like. The latter statement is very well applicable to bulges of early-type galaxies (e.g. Kormendy & Kennicutt 2004, Fisher & Drory 2008), but is not so obvious for late-type spirals. It implies that some late-type spirals have old bulges, that do not follow exponential distributions. Maybe our Milky Way galaxy has a bulge similar to those. We also see that n decreases for increasing star formation time scale τ . Late-type spiral disks, like the disk of our Milky Way, have long star formation time scales. As a result, parameters such as $H\beta$, which are strongly influenced by the last burst of star formation, generally show large values, indicative of the presence of young stellar populations. We find that galaxies with small star formation time scales, i.e. elliptical-like objects, have high n -values. Interesting are also the correlations with disk scale length. If there are signs of younger populations in the center, or if the star formation time scale is long, then the disks are generally smaller. This effect is probably due to the fact that more massive galaxies generally are of earlier-type, having a shorter star formation time scale, and show older bulges.

6.3 Trends between structural parameters

Coming to the relations among the structural parameters themselves, in Fig. 11 we plot the size and surface brightness of the bulges and disks of our galaxies against each other, and add the samples of GW and Fisher & Drory (2008) on the right: in the left panel we plot the central surface brightness of the disk against the effective surface brightness of the bulge; in the right one, disk scale length against bulge effective radius. We see a strong trend that galaxies with brighter disks harbour brighter bulges, and a tendency for galaxies with larger disks to have larger bulges (see before). The figure shows conclusively that bulge and disk are related, and that e.g. high surface brightness bulges do not co-exist with low surface brightness disks and vice-versa. The figure suggests that disks do not form without affecting the bulge. If a disk is formed in a galaxy which already contains a bulge, its size and surface brightness is either determined by the mass distribution of the bulge, or the bulge adapts itself, implying that stars are being formed in this process. The strong correlation between $\mu_{e,Bulge}$ and $\mu_{0,Disk}$ seems to support the process of the formation of bulges through secular evolution of disks.

7 CENTRAL COMPONENTS

In recent years, several studies have shown that many spiral galaxies host in their innermost regions an extra component, distinguishable in the images and/or photometric profiles as an excess light above the (exponential) disk plus (Sérsic) bulge. Nuclei are common both in early- and late- type galaxies. Phillips et al. (1996) found unresolved bright nuclei in six out of 10 late-type spirals; Matthews & Gallagher (1997) noticed a compact star cluster in the centres of 10 very late-type spirals, within a program studying 49 objects; out of a sample of 77 Scd-Sm galaxies, Böker et al. (2002) detected a distinct component in 59 cases. In some of the late-type spirals, these clusters are the only prominent source within a few kiloparsecs from the centre. In earlier-types their detection is complicated by the presence of a luminous and extended bulge, but Carollo et al. (1998) showed that nuclear clusters are present also there. As already mentioned, Balcells et al. (2007a) found a central light excess in 90 percent of a sample of S0-Sbc galaxies

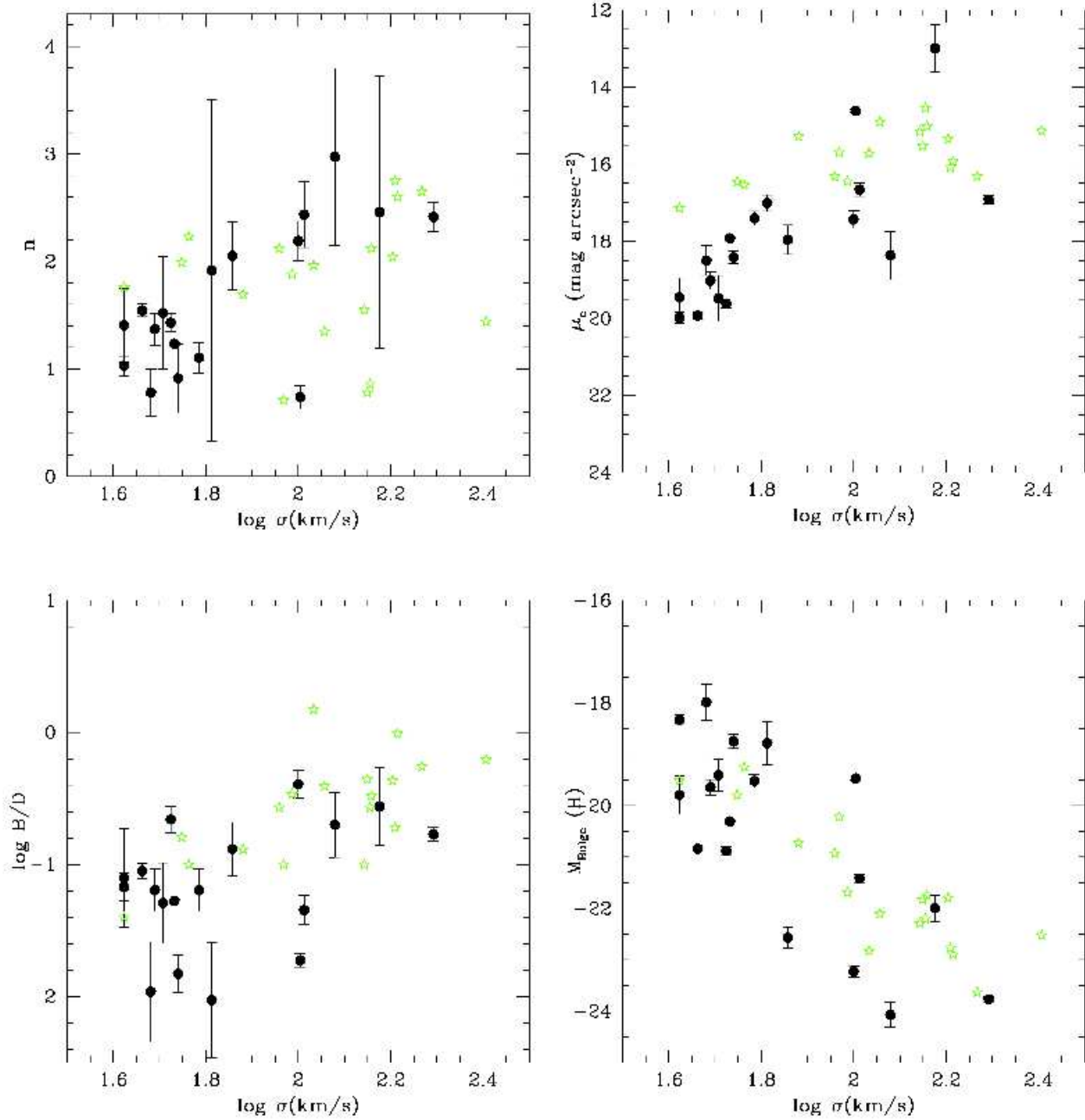


Figure 9. Structural parameters as a function of central stellar velocity dispersion for our late-type sample (black filled circles), compared to the sample of early-type spirals of Balcells et al. 2007b (green asterisks). The velocity dispersions for our sample are taken from Table 1 in Ganda et al. (2006). As for the morphological T-type, we have artificially put all the galaxies earlier than $T = 0$ in the sample of Balcells et al. 2007b to $T = 0$.

using NICMOS imaging, detecting both unresolved and extended sources; according to the authors, the extended inner components are geometrically flat systems and could be inner disks, rings or bars; the unresolved ones are most likely star clusters and are found in more than one third of the galaxies with inner component.

In our sample, two galaxies out of 18 (NGC 864 and NGC 4102) present a central depression and the remaining 16 show a central light excess above the best-fit to the bulge; one of these (NGC 5678) is an ambiguous case, possibly because of the very

extended dust lanes affecting this galaxy, but we included it in the ‘central component’ group. The numbers are very similar to those of Balcells et al. (2007a). Out of these 16, eight belong to the sample studied by Böker et al. (2002): all the Scd and Sd galaxies in our sample. The authors detect nuclear star clusters in all of them and publish an estimate of their size and luminosity in the I -band.

For all the 16 galaxies, we built model images of the bulges on the basis of the fit parameters, and subtracted them from the HST ‘bulge images’ (NICMOS or WFPC2-F814W depending on

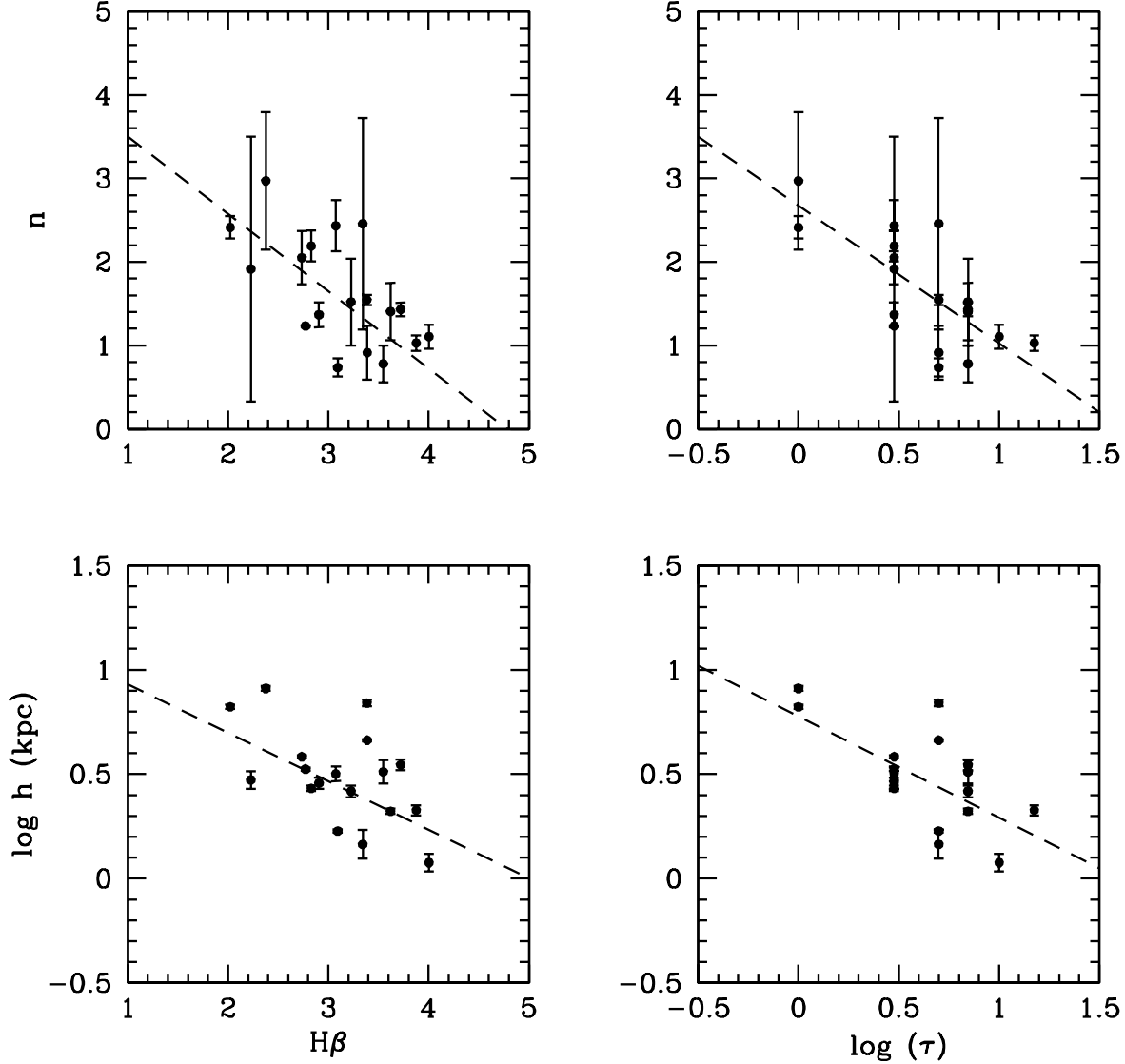


Figure 10. Correlations between the structural parameters n and disk scale length h as a function of stellar population parameters $H\beta$ (in Å) and star formation timescale τ (in Gyr). The dashed lines overlotted represent a linear fit to our data.

the object). The images that we obtained contain by construction the residuals from the global (exponential) disk + (Sérsic) bulge fit to the galaxy: dust features, spiral structure, bars, and the inner component in which we are interested. We estimated the HWHM of the central component using the IRAF `rimexam` task, resulting in values ranging between ≈ 0.07 and $0.23''$. We then calculated the flux enclosed in a circle of radius twice the HWHM and converted it to a magnitude scale (H – band). For NGC 4102 and NGC 864 we calculated the flux by measuring all the light in the inner aperture of diameter $0.227''$. The computed magnitudes (both apparent and absolute) are listed in Table 7, where an asterisk marks the galaxies

in common with the sample analysed by Böker et al. (2002). For all galaxies for which both HST F606W and F160W data are available, we also calculated the central $V - H$ colour in an aperture of diameter $0.227''$ ($0.500''$ for NGC 5585), and also tabulated these in Table 7. Fig. 12 shows the comparison between the apparent magnitudes that we calculated and those published by Böker et al. (2002), for the inner component of the galaxies in common. The magnitudes of Böker et al. refer to the I – band, while our data are H – band data (see Table 4). The only galaxy in common with Böker et al. (2002) is NGC 5585, which is representative for the galaxies in this group, and clearly shows much less extinction in its $V - H$ color

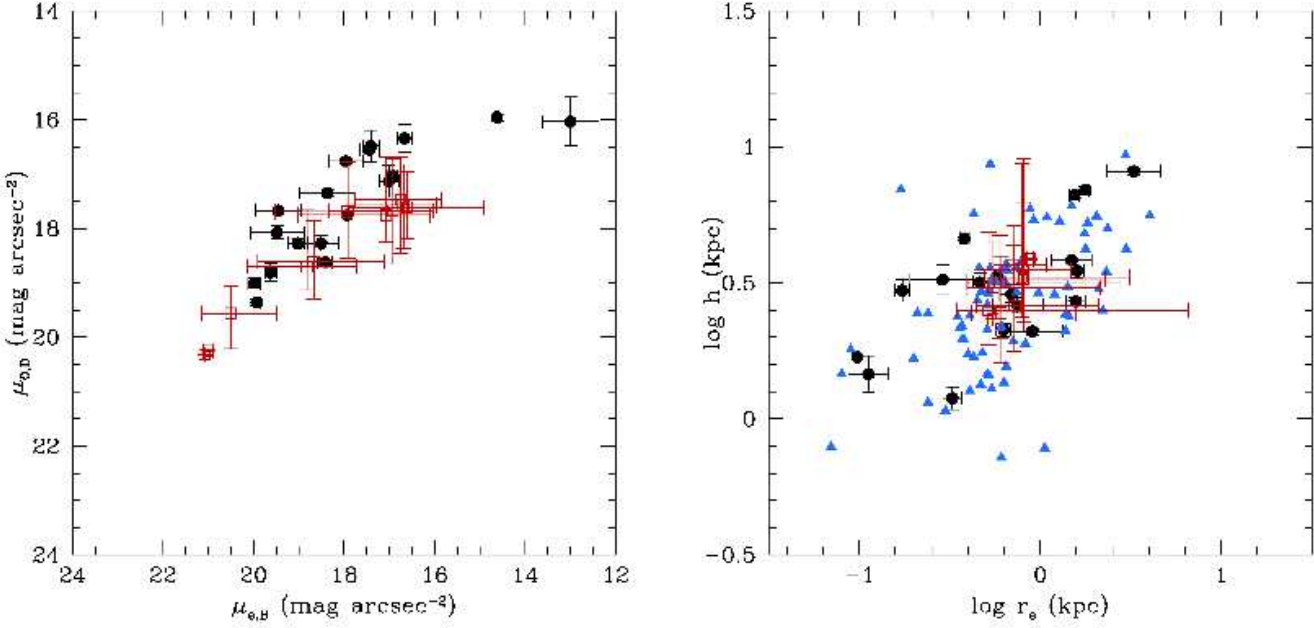


Figure 11. Bulge against disk parameters: *left panel:* disk central brightness $\mu_{0, Disk}$ against bulge effective surface brightness $\mu_{e, Bulge}$ measured in mag arcsec^{-2} ; *right panel:* disk scale length h against bulge effective radius r_e , both measured in kpc. Filled dots are the galaxies of this paper. Blue triangles are galaxies from Fisher & Drory (2008), while the open red squares indicates the compilation of Graham & Worley (2008).

map. We also see that the $V - H$ colors of the nuclei are similar within 0.2 mag to the colors in the inner aperture with diameter $2.4''$ ($\Delta((V - H)_c - (V - H)_{nuc}) = -0.007 \pm 0.199 \text{ mag}$). Even though only about 10% of the light in the larger aperture comes from the nuclear cluster, it shows that the stellar populations of the nuclear cluster are not decoupled from those in the rest of the galaxy, as is e.g. the case in globular clusters in galaxies.

Walcher et al. (2006) took high resolution spectra for a number of the Scd, Sd and Sm galaxies of Böker et al. (2002) and analysed them using stellar population synthesis, allowing the extinction to be fitted as a free parameter. They find an average extinction in I of $\sim 0.4 \text{ mag}$, which is very comparable to what we find ($A_V = 0.68$, with a scatter of 0.55): When using the Galactic extinction law (Rieke & Lebofsky 1985) the extinction in V is $1.64 \times$ the extinction in I_C , or 0.66 mag. Given the fact that the galaxies of Walcher et al. are later type than ours, we expect less extinction than in our sample. However, large variations probably exist from galaxy to galaxy, and also the amount of extinction that one obtains varies with method. We can only conclude that extinction is important in late-type galaxies. Note that NGC 1042, in common with our paper, has by far the largest extinction ($A_I = 1.35 \text{ mag}$), consistent with Figure 12.

8 SUMMARY AND CONCLUSIONS

In this Paper we performed a photometric bulge-disk decomposition for our sample of 18 late-type spiral galaxies. We used NIR ($H -$ band) archive images (DSS, 2MASS and HST) from which we retrieved photometric profiles covering the whole disk and having a high spatial resolution in the inner parts. We fitted an exponential disk and a Sérsic bulge, using a method that allows the two

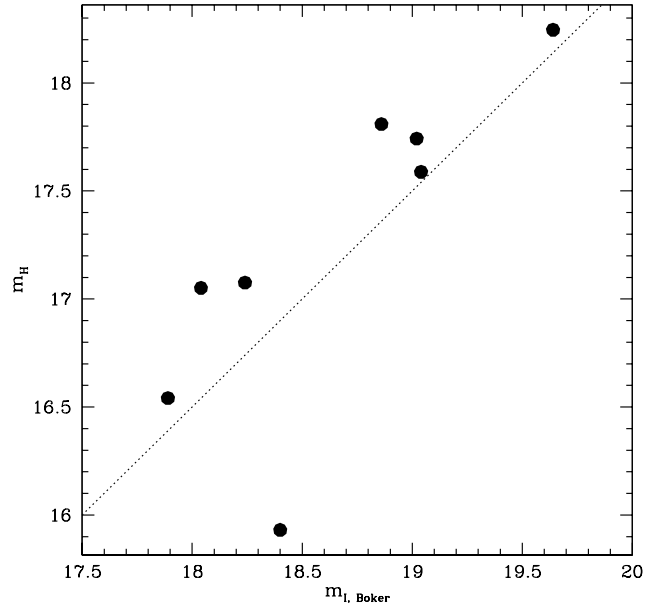


Figure 12. Apparent magnitude of the inner component against those published by Böker et al. (2002). The solid line overplotted indicates the $I = H + 1.5$ line. The clear outlier below the solid line represents NGC 1042.

components to have different intrinsic shapes, but without going to a full two-dimensional fitting of the light distribution; we studied in detail the correlations between the fit parameters, and we investigated the high resolution $V - H$ colours in this sample, in the nuclear cluster and outside it. From the $V - H$ colour maps and

x	y	c	x	y	c
(1)	(2)	(3)	(4)	(5)	(6)
T	n	-0.599	$\log(\sigma)$	n	0.641
T	$\mu_{e,b}$	0.769	$\log(\sigma)$	$\mu_{e,b}$	-0.742
T	$\log(r_e)$	0.155	$\log(\sigma)$	$\log(r_e)$	0.028
T	$\mu_{0,d}$	0.843	$\log(\sigma)$	$\mu_{0,d}$	-0.720
T	$\log(h)$	0.045	$\log(\sigma)$	$\log(h)$	0.113
T	r_e/h	0.150	$\log(\sigma)$	r_e/h	-0.065
T	$\log(B/D)$	-0.256	$\log(\sigma)$	$\log(B/D)$	0.416
M_d	n	-0.679	M_b	n	-0.705
M_d	$\mu_{e,b}$	0.394	M_b	$\mu_{e,b}$	0.276
M_d	$\log(r_e)$	-0.297	M_b	$\log(r_e)$	-0.567
M_d	$\mu_{0,d}$	0.490	M_b	$\mu_{0,d}$	0.416
M_d	$\log(h)$	-0.555	M_b	$\log(h)$	-0.414
M_d	r_e/h	-0.022	M_b	r_e/h	-0.483
M_d	$\log(B/D)$	-0.260	M_b	$\log(B/D)$	-0.794
$H\beta$	n	-0.681	$H\beta$	$\log(h)$	-0.532
$\Delta Mgb'$	$\log(r_e)$	0.724	$\Delta Mgb'$	$\log(h)$	0.759
$\log(\tau)$	n	-0.678	$\log(\tau)$	$\log(h)$	-0.633
M_{Bulge}	$\log(\sigma)$	-0.756	M_{Bulge}	T	0.630
$\mu_{e,b}$	$\mu_{0,d}$	0.866	$\log(r_e)$	$\log(h)$	0.693
n	$\mu_{0,d}$	-0.430	n	$\mu_{e,b}$	-0.338
n	$\log(h)$	0.285	n	$\log(r_e)$	0.231
n	r_e/h	0.143	n	$\log(B/D)$	0.440

Table 5. Correlation coefficient c for the parameter-parameter relations, for our sample only. We report the correlation coefficient for all the relations of Figs. B1.a and b, and B2.a and b; for those of Figs. B3 we only list those with $|c| \geq 0.5$. Columns (1), (2) and (4), (5): variables; columns (3) and (6): correlation coefficient. For the relations involving the T-type, all the individual points are considered and not the average values within a type (as done instead in Fig. B1.a and b).

x	y	a	b	x	y	a	b
(1)	(2)	(3)	(4)	(5)	(6)	(7)	(8)
T	n	3.104	-0.287	$\log(\sigma)$	n	-2.654	2.332
T	$\mu_{e,b}$	14.644	0.688	$\log(\sigma)$	$\mu_{e,b}$	30.036	-6.628
T	$\mu_{0,d}$	14.346	0.623	$\log(\sigma)$	$\mu_{0,d}$	24.903	-4.017
M_d	n	-7.970	-0.410	M_b	n	-4.941	-0.316
M_d	$\log(h)$	-2.045	-0.108	M_b	$\log(r_e)$	-2.936	-0.133
				M_b	$\log(B/D)$	-5.292	-0.200
$H\beta$	n	4.329	-0.876	$H\beta$	$\log(h)$	1.157	-0.221
$\Delta Mgb'$	$\log(r_e)$	0.353	14.966	$\Delta Mgb'$	$\log(h)$	0.807	8.358
$\log(\tau)$	n	2.638	-1.590	$\log(\tau)$	$\log(h)$	0.782	-0.481
M_{Bulge}	$\log(\sigma)$	0.190	-0.081	M_{Bulge}	T	15.442	0.506
$\mu_{e,b}$	$\mu_{0,d}$	8.092	0.527	$\log(r_e)$	$\log(h)$	0.566	0.373

Table 6. Parameters of the linear best-fit for the relations with $|c| \geq 0.5$ in Table 5. The relation $y = a + b \times x$, with y and x variables (columns (1), (2), (5), (6)) and a and b fit parameters (columns (3), (4), (7), (8)) is fitted to the data for our sample only. For the relations involving the T-type, all the individual points are considered and not the average values for the same type (as done instead in Fig. B1.a and b).

NGC	m_{inner}	M_{inner}	$V - H$
(1)	(2)	(3)	(4)
488	14.10	-18.44	3.196
628	16.27	-13.68	2.644
772	14.30	-18.46	
864	16.86	-13.02	2.863
1042*	15.93	-15.35	
2805*	17.74	-14.51	
2964	15.45	-16.12	3.496
3346*	18.25	-13.14	
3423*	17.59	-13.25	
3949	17.10	-13.71	2.695
4030	16.19	-15.42	3.027
4102	15.07	-15.55	3.499
4254	15.60	-15.84	3.271
4487*	16.54	-14.29	
4775*	17.05	-14.71	
5585*	17.08	-12.50	2.281
5668*	17.81	-14.08	
5678	15.77	-16.71	3.657

Table 7. Column (1): NGC identifier of the galaxies with measurable inner component; columns (2): apparent magnitude m_{inner} of the inner component, in $H -$ band; columns (3): absolute magnitude M_{inner} of the inner component, in $H -$ band. Columns (4): Central colours in apertures of 0.227'' diameter (0.500'' for NGC 5585) for the galaxies with both HST F606W and F160W data. The asterisks marks the galaxies in common with the sample of Böker et al. (2002).

the Mg b maps of Ganda et al. (2007) we made extinction maps for 10 of the galaxies. We summarize below the main results.

- Late-type spirals can be fitted well by a model consisting of a Sérsic bulge, an exponential disk, and a nuclear light access. Outside the central regions, the bulk of the galaxy's light is well described by one exponential disk, although in some cases a double exponential (inner + outer disk) would provide better fits, as tested by Pohlen & Trujillo (2006). In most cases bulges are rounder than their disks, but for the latest types the opposite sometimes holds, possibly in relation with the presence of a bar.

- Bulges of late-type spiral galaxies follow the same relation between central velocity dispersion and bulge luminosity as bulges of early-type spirals. This might indicate that the black hole - sigma relation also holds for late-type spiral bulges. Late-type bulges have, however, lower surface brightness and are larger than early-type bulges.

- The structural parameters of our bulges agree statistically with the large compilation of Graham & Worley (2008), showing a strong correlation between surface brightness of bulge and disk, and a less strong relation between bulge effective radius and disk scale length.

- The star formation time scale inversely correlates with the Sérsic index n , implying that exponential bulges have long star formation time scales, in agreement with the prediction from secular evolution models, that exponential bulges are disks forming through secular evolution.

- In 16 out of 18 galaxies the galaxy's profile presents an excess light with respect to the fitted disk + bulge, which can be interpreted as an additional tiny component, in many cases (in all the later types) a nuclear star cluster. We give an estimate of the magnitude of these inner components.

- Using $V - H$ colour maps from HST imaging and SAURON Mg b maps, we have determined model-independent extinction

maps for 10 of the 18 galaxies. We find that the central A_V ranges from 0 to 2 mag, with many galaxies being optically thick in the optical. The $V - H$ profiles show a lot of structure, mostly due to extinction, with much larger gradients than are generally displayed by early-type galaxies.

- The colours of nuclear clusters are the same as the inner regions of their host galaxies, with a scatter of 0.2 mag, indicating a similar composition and age as the stellar populations just outside the center, unlike e.g. galactic globular clusters.

ACKNOWLEDGEMENTS

We thank Alessandro Boselli and Luca Cortese for kindly making available profiles useful in establishing the reliability of the methods used in this Paper. We also thank Leslie Hunt, who very gently provided us her data in tabular format, and Michael Pohlen, who provided us his profiles as well. We kindly acknowledge Edo Noor-dermeer for very useful discussions and both him and Alister Graham for providing FORTRAN codes used in the preparation of the present Paper. Thanks to Isabel Pérez, Gert Sikkema and Michele Cappellari for helpful discussions and suggestions. KG acknowledges support for the Ubbo Emmius PhD program of the University of Groningen. This project made use of the HyperLeda and NED databases. Part of this work is based on data obtained from the STSci Science Archive Facility. The Digitized Sky Surveys were produced at the Space Telescope Science Institute under U.S. Government grant NAGW-2166. The images of these surveys are based on photographic data obtained using the Oschin Schmidt Telescope on Palomar Mountain and the UK Schmidt Telescope.

APPENDIX A: INTERNAL CONSISTENCY OF THE METHOD - LITERATURE COMPARISON

In order to ensure the reliability of the method applied, we searched the literature for published $H -$ band profiles. For the late-type spiral galaxies of our sample extremely little is available. One of the few existing references is the work of Hunt & Malkan (2004), who present NICMOS photometry for 250 active and normal galaxies, among which six are in common with our sample: NGC 488, 772, 2964, 3949, 4102, 5678. In almost all cases they used the same images as we did. The authors were so kind to provide us in tabular format the profiles for those galaxies, that they extracted keeping the centre of the isophotes fixed, but allowing the geometric parameters to vary over the whole radial range. In order to match their approach, we extracted again photometric profiles from the 2MASS and NICMOS images (DSS profiles are here redundant, since the literature profiles are available only in the inner $\approx 10''$ only; therefore we did not use them) along the average position angle and ellipticity of the profiles from Hunt & Malkan (2004). In Fig. A1 we show for those six galaxies the comparison with Hunt & Malkan (2004): the profiles (left panels) and the difference between them, plotted on the common radial range. The agreement is satisfactory (see also figure caption). NICMOS profiles for five of the six galaxies in common with Hunt & Malkan (2004) (NGC 488, 772, 2964, 3949, 5678), again derived from the same images that we used, are published also by Seigar et al. (2002); from a visual inspection of their profiles, we noticed that there is a significant offset with ours and Hunt's profiles, which is probably due to the adoption of another magnitude system (AB

magnitude system), therefore we did not proceed to a more detailed comparison.

As a reference for the ground-based $H -$ band photometry, we chose to use the work of Gavazzi et al. (2001), who present $H -$ band observations and surface brightness profile decomposition for 75 faint galaxies, mostly dwarf ellipticals belonging to the Virgo cluster. They collected $H -$ band images at the ESO-NTT telescope in La Silla (Chile) and at the TNG on La Palma (Spain), reduced and calibrated the images and extracted brightness profiles fitting ellipses with ellipse centres, ellipticities and position angles left as free parameters. This corresponds to the first step in our procedure, as we described above. Since there is no overlap between their sample and ours, we chose some galaxies out of their paper (NGC 4353, 4440, 4600, 4706 and 4743), retrieved the 2MASS and DSS images for these galaxies and extracted brightness profiles with free geometric parameters, subtracted an estimate for the sky background, combined them into a single profile and converted the latter to an absolute magnitude scale in the same way as done for our own galaxies -we only skipped the steps where we fix the geometric parameters, for consistency with the approach used by Gavazzi et al. (2001). Fig. A2 shows for the chosen galaxies the comparison between our profiles and those published by Gavazzi et al. (2001), kindly made available in tabular format by the authors. The figure shows that the agreement is good, confirming the reliability of our method.

APPENDIX B: STRUCTURAL PARAMETER RELATIONS

In this appendix we present a large number of relations, between structural parameters and luminosity of bulge, disk and total galaxy, and between structural and stellar population parameters. A few of these have already been discussed in Section 5. For the relations between structural parameters and luminosity of bulge, disk and total galaxy we find that our late type spiral galaxies generally behave in the same way as the compilation of Graham & Worley (2008). In Section 5.1 and 5.2 the most important correlations were discussed. Here we discuss more relations, for completeness.

We start looking at the relations between the structural parameters of bulge and disk and global galaxy properties such as morphological type and velocity dispersion. We plot these parameters against each other in Fig. B1.a and B1.b, for our sample with the compilation of GW always plotted as well to guide the eye. If we focus on our sample only, we can notice some trends: n tends to decrease going to later types, and both the effective surface brightness of the bulge and the central surface brightness of the disk decrease going to later types. These correlations agree with GW and B07. Interesting to note is that for galaxies earlier than Sbc surface brightness of bulge and disk is virtually independent of type. For later types there is a strong correlation. There galaxies become smaller, and have lower surface brightness of both bulge and disk, for increasing morphological type (see also de Jong 1996, paper III). We confirm that there is no strong correlation between the size of bulges and disk and morphological type. Also, the size ratio r_e/h is independent of type, and we do not find the mild decrease that MacArthur et al. (2003) claim. See GW for an extended discussion about this ratio. The most important correlations with central velocity dispersion have been discussed in Section 5.1. We find that the effective radius of the bulge does not correlate with σ , nor does the scale length of the disk, or the ratio of bulge effective radius to disk scale length. There is a good correlation between bulge luminosity and σ (see also B07) and between bulge to disk ratio and σ .

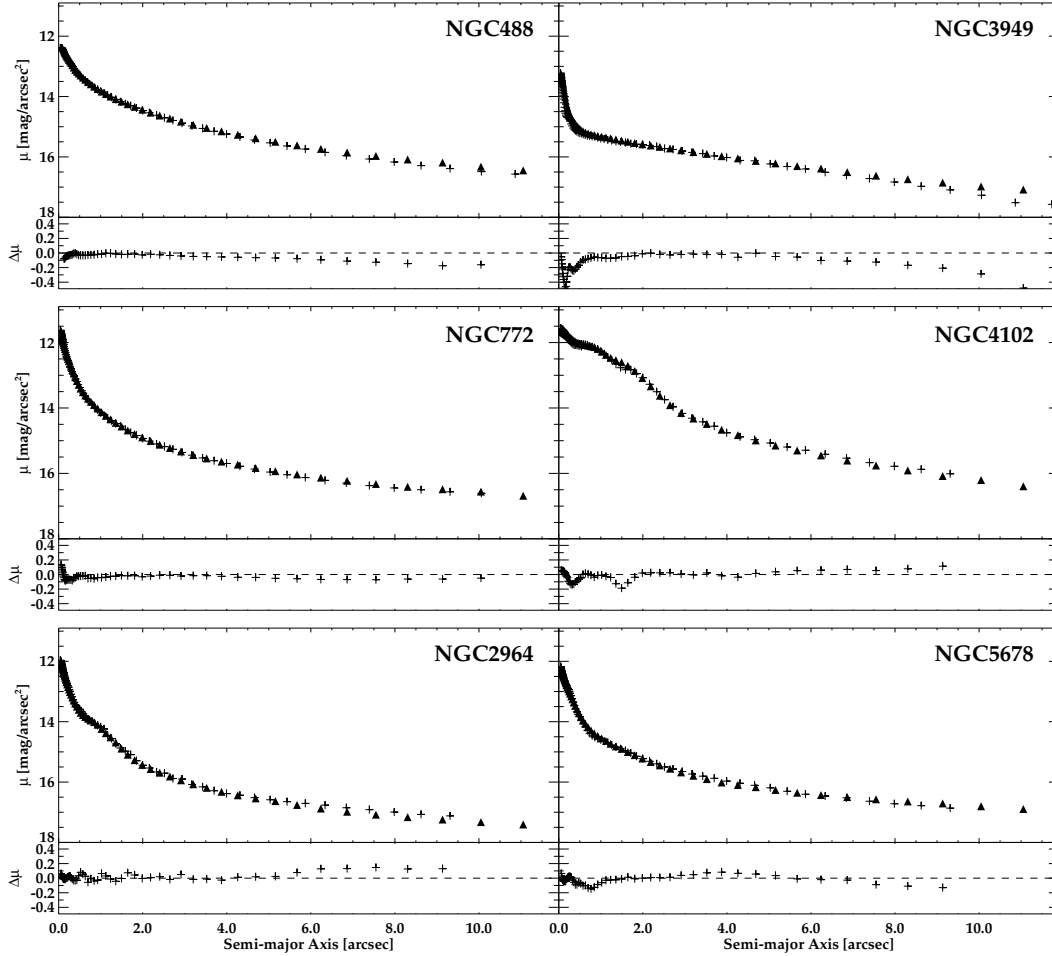


Figure A1. Comparison between our combined NICMOS + 2MASS profiles and the profiles published by Hunt & Malkan (2004) for the six galaxies in common, plotted on the common radial range. In the left panels, the crosses represent our profiles, and the filled triangles those kindly made available by Leslie Hunt, also plotted on the common radial range. In the right panels, we plot the difference between the two. The difference is relevant only in the innermost $0.1\text{--}0.3''$, and might be due to small differences in the centering and/or in the geometric parameters. In particular, NGC 3949 represents the case with the largest difference in the innermost points, and it is also the case where the difference between the ellipticity profile from Hunt and the mean value we adopted is the largest.

In Fig. B2.a and B2.b we plot the structural parameters of bulges and disks as a function of bulge, disk and total H -band luminosity. We see that surface brightness of bulges and disks increases with increasing bulge or disk luminosity, consequence of the constancy of disk scale length and bulge effective radius. Since later type spiral galaxies tend to be fainter, we find that the shape parameter n increases with the luminosity of the bulge, disk or the whole galaxy. The relation between the bulge magnitude M_b and n (top right panel in Fig. B2.a) is particularly tight: the correlation coefficient c is ≈ -0.7 , and it becomes even tighter ($c \approx -0.92$) when removing the outlier point representing NGC 864. As shown by B07 in their Figure 6c, spiral galaxies follow the same trend as the Virgo ellipticals from Caon, Capaccioli & D’Onofrio (1993) in the plane (M_{Bulge}, n). We find a marginally significant correlation between bulge luminosity and effective radius, in the sense that brighter bulges are also larger. When the whole compilation of GW is considered this correlation is not found. In general, when the bulge luminosity increases, the Sérsic index n decreases, and the surface brightness increases, with constant effective radius. For

late type spirals only, which all have a similar Sérsic index ($n=1$), there is apparently a tendency that both μ_e and r_e increase. The marginally significant correlation between disk luminosity and disk scale length is probably caused by the two bright outliers. The B/D luminosity ratio increases as galaxy bulges become more luminous, while it does not show strong trends with the disk magnitude M_{Disk} . In general, from this work we infer that several correlations between structural properties of spiral galaxies are tighter versus M_{Bulge} than versus M_{Disk} (see Table 5), in agreement with the conclusion of Balcells et al. (2007b). This is particularly intriguing, implying that (some of) the properties are driven by the mass of the bulge. GW, who find the same strong relation, also comment that these new decompositions, with Sérsic rather than de Vaucouleurs bulge, show that very few spirals have $B/T > 1/3$. In a long discussion GW confirm this conclusion, and point out that the B/D ratios in cosmological galaxy simulations are on the average much larger, showing that the models, or probably the recipes for supernova feedback, need to be improved considerably.

Fig. B3 shows the Sérsic parameter n , the bulge effective sur-

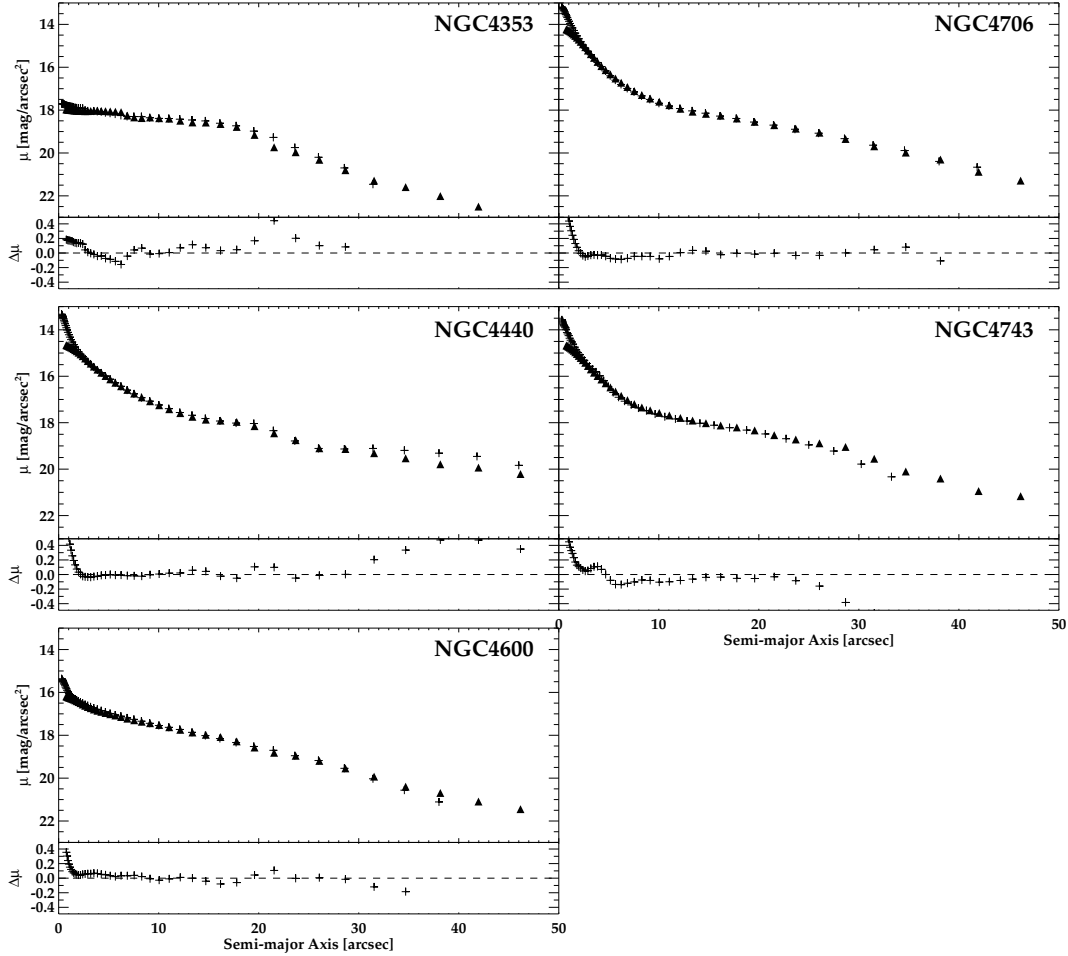


Figure A2. Comparison between the combined 2MASS-DSS profiles and the profiles from Gavazzi et al. (2001) for five galaxies taken from Gavazzi et al. (2001, see text for a more detailed description). In the left panels, the crosses represent our profiles, the filled triangles those from Gavazzi et al. (2001); the vertical scale is in absolute H magnitudes arcsec^{-2} . In the right panels, we show on the common radial range the difference in magnitudes arcsec^{-2} between the profiles from Gavazzi et al. (2001) and ours. In most cases, the differences are significant (more than $0.1 \text{ mag arcsec}^{-2}$) only in the innermost $2\text{--}3''$, where our 2MASS profiles are affected by seeing smearing much more than the ones of Gavazzi et al. (2001), and at radii larger than $25\text{--}30''$, corresponding to the external limit of the profiles from Gavazzi et al. (2001). This proves that the agreement is good.

face brightness and radius, the disk central surface brightness and scale length, the r_e/h ratio and the B/D luminosity ratio as a function of $H\beta$, $\Delta Mgb'$, age and star formation time-scale τ . The stellar population parameters refer to a central aperture of radius $1''.5$. $\Delta Mgb'$ is the difference in magnitudes between the observed Mgb index and the prediction, based on the observed velocity dispersion, given by the $Mg_2 - \sigma$ relation published by Jørgensen et al. (1996), which is now believed to hold for old spheroids (see discussion in Peletier et al. (2007)); $\Delta Mgb'$ is therefore a measure of the importance of young populations in the galaxy. For the sake of clarity, we remind the reader that $\Delta Mgb'$ can be derived from Mgb and σ in the following way, adopting the $Mg_2 - \sigma$ relation from Jørgensen, expressed as in Eq. 3 in the paper of Ganda et al. (2007), the definition of Mgb' inferred from Eq. 2 in the same paper and the conversion between Mg_2 and Mgb' given in Eq. 4 there:

$$\Delta Mgb' = -2.5 \times \log(1 - Mgb/32.5) - 0.096 \times \log(\sigma) + 0.062. \quad (\text{B1})$$

Going back to Fig. B3 and to the description of the quantities involved here, the age is the Single Stellar Population (SSP)-equivalent age inferred by comparison of observed line-strength in-

dicies with models and τ is the e -folding time-scale for star formation, assuming a galaxy age of 10 Gyr and an exponentially declining star formation rate with time. For details we refer the reader to Sections 5.3, 6.1 and 6.3, in Ganda et al. (2007). We can observe some trends, a few of which significant ($|c| \geq 0.5$), in those cases we have also plotted the correlation as a dashed line: when $H\beta$ increases, i.e. when the stellar population becomes younger, n decreases, both $\mu_{0, \text{Disk}}$ and $\mu_{e, \text{Bulge}}$ become fainter, and the disk scale length h and the bulge effective radius r_e decrease. There are also indications that both r_e and h become smaller with $\Delta Mgb'$ becoming more negative, which means that galaxies farther away from the $Mg_2 - \sigma$ relation of old ellipticals, i.e. younger galaxies, have both smaller bulges and smaller disks. No relevant trend is found with age: possibly a confirmation of the fact that, in general, SSP-equivalent ages and metallicities are not a good approximation for spiral galaxies, as discussed by Peletier et al. (2007) and Ganda et al. (2007). A more relevant parameter for our galaxies seems to be τ , in the framework of a continuous star formation: as τ increases (and the star formation history is less and less well

described by a single burst), n becomes smaller, $\mu_{0,d}$ and $\mu_{e,b}$ become fainter and r_e and h become smaller. No significant trend is observed involving the ratio r_e/h ratio and the B/D luminosity ratio. Globally, Fig. B3 seem to corroborate a scenario where galaxies with a quiescent, almost constant star formation, hosting composite stellar populations, with (at least) some young stars, have almost-exponential bulges and small and faint bulges and disks, while galaxies that formed stars in a single burst long ago (more SSP-like) tend to have higher n and bigger and brighter bulges and disks. A similar scenario, in which the character of the star formation history is replaced by the galaxy age, is suggested also by Hunt, Pierini & Giovanardi (2004), as we mentioned earlier: exponential bulges would be young products of secular evolution; as the galaxy ages, the bulges would grow and their n increase.

References

- Aguerri J.A.L., Balcells M., Peletier R.F., 2001, *A&A*, 367, 428
 Andredakis Y., Sanders R., 1994, *MNRAS*, 267, 283
 Andredakis Y.C., Peletier R.F., Balcells M., 1995, *MNRAS*, 275, 874
 Bacon R. et al., 2001, *MNRAS*, 326, 23 (Paper I)
 Balcells M., Graham A.W., Peletier R.F., 2007a, *ApJ*, 665, 1084
 Balcells M., Graham A.W., Peletier R.F., 2007b, *ApJ*, 665, 1104
 Böker T., Laine S., van der Marel R.P., Sarzi M., Rix H.-W., Ho L.C., Shields J.C., 2002, *AJ*, 123, 1389
 Boroson T., 1981, *ApJS*, 46, 177
 Boroson T., Strom K.M., Strom S.E., 1983, *ApJ*, 274, 39
 Boselli, A., & Gavazzi, G. 1994, *A&A*, 283, 12
 Bruzual, G., & Charlot, S. 2003, *MNRAS*, 344, 1000
 Caon N., Capaccioli M., D’Onofrio M., 1993, *MNRAS*, 265, 1013
 Carollo C.M., Stiavelli M., de Zeeuw P.T., Mack J., 1997, *AJ*, 114, 2366
 Carollo C.M., Stiavelli M., 1998, *AJ*, 115, 2306
 Carollo C.M., Stiavelli M., Mack J., 1998, *AJ*, 116, 68
 Carollo C.M., 1999, *ApJ*, 523, 566
 Carollo, C. M., Stiavelli, M., de Zeeuw, P. T., Seigar, M., & Dejonghe, H. 2001, *ApJ*, 546, 216
 Carollo C.M., Stiavelli M., Seigar M., de Zeeuw P.T., Dejonghe H., 2002, *AJ*, 123, 159
 Carollo, C. M., Scarlata, C., Stiavelli, M., Wyse, R. F. G., & Mayer, L. 2007, *ApJ*, 658, 960
 Ciotti L., Bertin G., 1999, *A&A*, 352, 447
 Combes F., Debbasch F., Friedli D., Pfenniger D., 1990, *A&A*, 233, 82
 Courteau S., de Jong R., Broeils, 1996, *ApJ*, 457, L73
 de Jong R.S., van der Kruit P.C., 1994, *A&AS*, 106, 451
 de Jong R.S., 1995, PhD Thesis, Univ. Groningen
 de Jong R.S., 1996a, *A&AS*, 118, 557
 de Jong R.S., 1996b, *A&A*, 313, 45
 de Vaucouleurs G., 1948, *Ann.D’Astroph.*, 11, 247
 de Vaucouleurs, G. 1959, *ApJ*, 130, 728
 de Vaucouleurs G., de Vaucouleurs A., Corwin H.G.Jr., Buta R.J., Paturel G., Fouqué P., 1991, *Third Reference Catalogue of Bright Galaxies*, Springer-Verlag, New York (RC3)
 de Zeeuw P.T. et al., 2002, *MNRAS*, 329, 513 (Paper II)
 D’Onofrio M., Capaccioli M., caon N., 1994, *MNRAS*, 271, 523
 Driver, S. P., Popescu, C. C., Tuffs, R. J., Liske, J., Graham, A. W., Allen, P. D., & de Propriis, R. 2007, *MNRAS*, 379, 1022
 Erwin, P., & Sparke, L. S. 2002, *AJ*, 124, 65
 Erwin P., Beltrán J.C.V., Graham A.W., Beckman J.E., 2003, *ApJ*, 597, 929
 Falcón-Barroso, J., et al. 2006, *MNRAS*, 369, 529
 Fathi K., Peletier R.F., 2003, *Astron.Astrophys.*, 407, 61
 Ferrarese, L., & Merritt, D. 2000, *ApJ*, 539, L9
 Fisher, D. B., & Drory, N. 2008, *AJ*, 136, 773
 Freeman K.C., 1970, *ApJ*, 160, 811
 Frogel, J. A., Persson, S. E., Matthews, K., & Aaronson, M. 1978, *ApJ*, 220, 75
 Frogel J.A., 1985, *ApJ*, 298, 528
 Ganda K., Falcón-Barroso J., Peletier R.F., Cappellari M., Em-sellem E., McDermid R., de Zeeuw P.T., Carollo M., 2006, *MNRAS*, 367, 46
 Ganda K. et al., 2007, *MNRAS*, 380, 506
 Gavazzi G., Zibetti S., Boselli A., Franzetti P., Scodreggio M., Martocchi S., 2001, *A&A*, 372, 29
 Gebhardt, K., et al. 2000, *ApJ*, 543, L5
 Giovanardi C. & Hunt L.K., 1988, *AJ*, 95, 408
 Giovanelli, R., Haynes, M. P., Salzer, J. J., Wegner, G., da Costa, L. N., & Freudling, W. 1995, *AJ*, 110, 1059
 Graham A.W., 2001, *AJ*, 121, 820
 Graham, A. W., & Driver, S. P. 2007, *ApJ*, 655, 77
 Graham, A. W., & Driver, S. P. 2005, *Publications of the Astronomical Society of Australia*, 22, 118
 Graham, A. W., & Worley, C. C. 2008, *MNRAS*, 388, 1708
 Grosbøl P.J., 1985, *A&AS*, 60, 261
 Holtzman J.A., Borrows C.J., Casertano S., Hester J.J., Trauger J.t., Watson A.M., Worthey G., 1995, *PASP*, 107, 1065
 Hunt L.K., Malkan M.A., 2004, *ApJ*, 616, 729
 Hunt L.K., Pierini D., Giovanardi C., 2004, *A&A*, 414, 905
 Jedrzejewski R.I., 1987, *MNRAS*, 226, 747
 Jørgensen I., Franx M., Kjaergaard P., 1996, *MNRAS*, 280, 167
 Kent S.M., 1983, *ApJ*, 226, 562
 Kent S.M., 1984, *ApJS*, 56, 105
 Kent S.M., 1985, *ApJS*, 59, 115
 Kent S.M., 1986, *AJ*, 91, 1301
 Knapen, J. H., Beckman, J. E., Shlosman, I., Peletier, R. F., Heller, C. H., & de Jong, R. S. 1995, *ApJ*, 443, L73
 Kormendy J., 1977, *ApJ*, 217, 406
 Kormendy J., Illingworth G., 1982, *ApJ*, 256, 460
 Kormendy, J. 1993, *Galactic Bulges*, 153, 209
 Kormendy J., Kennicutt R.C.Jr., 2004, *ARA&A*, 42, 603
 Kuchinski, L. E., Terndrup, D. M., Gordon, K. D., & Witt, A. N. 1998, *AJ*, 115, 1438
 Kuntschner, H., et al. 2006, *MNRAS*, 369, 497
 Laine S., Shlosman I., Knapen J.H., Peletier R.F., *ApJ*, 567, 92
 MacArthur L., Courteau S., Holtzmann J., 2003, *ApJ*, 582, 689
 MacArthur, L. A. 2005, *ApJ*, 623, 795
 Martini, P., Regan, M. W., Mulchaey, J. S., & Pogge, R. W. 2003, *ApJ*, 589, 774
 Matthews L.D., Gallagher J.S.III, 1997, *AJ*, 114, 1899
 Möllenhoff C., Heidt J., 2001, *A&A*, 368, 16
 Moriondo G. et al., 2001, *A&A*, 370, 881
 Moriondo G., Giovanardi C., Hunt L.K., 1998, *A&AS*, 130, 81
 Noordermeer E., 2006, PhD Thesis, Univ. Groningen
 Noordermeer E., van der Hulst J.M., 2007, *MNRAS*, 376, 1480
 Norman C., Sellwood J.A., Hasan H., 1996, *ApJ*, 462, 114
 Palunas P., Williams T.B., 2000, *AJ*, 120, 2884
 Peletier, R. F., Valentijn, E. A., & Jameson, R. F. 1990, *A&A*, 233, 62
 Peletier, R. F., Valentijn, E. A., Moorwood, A. F. M., Freudling, W., Knapen, J. H., & Beckman, J. E. 1995, *A&A*, 300, L1

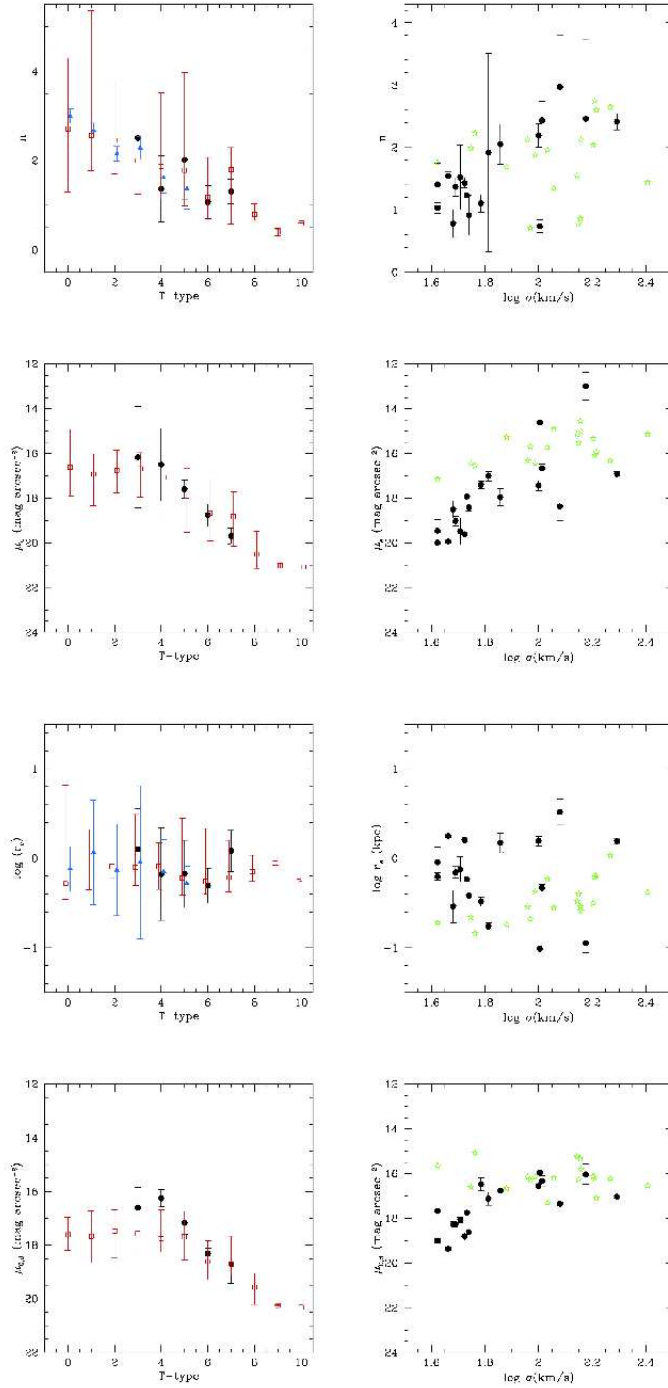


Figure B1.a. Bulge and disk structural parameters as a function of morphological T-type and central stellar velocity dispersion σ . The black filled circles represent our sample; blue triangles represent the sample of Fisher & Drory (2008). The red open squares represent the literature compilation of Graham & Worley (2008). *Left panels:* from top to bottom we plot n , $\mu_{e,Bulge}$, r_e and $\mu_{0,Disk}$; for each sample and each value of T-type, we plot the average value of the quantity of interest for all the galaxies of that type in that sample, with an errorbar indicating the standard deviation around the mean. *Right panels:* we plot the same quantities against $\log(\sigma)$, measured in km s^{-1} . The velocity dispersions for our sample are taken from Table 1 in Ganda et al. (2006). As for the morphological T-type, we have artificially put all the galaxies earlier than T = 0 in the sample of Balcells et al. 2007b to T = 0.

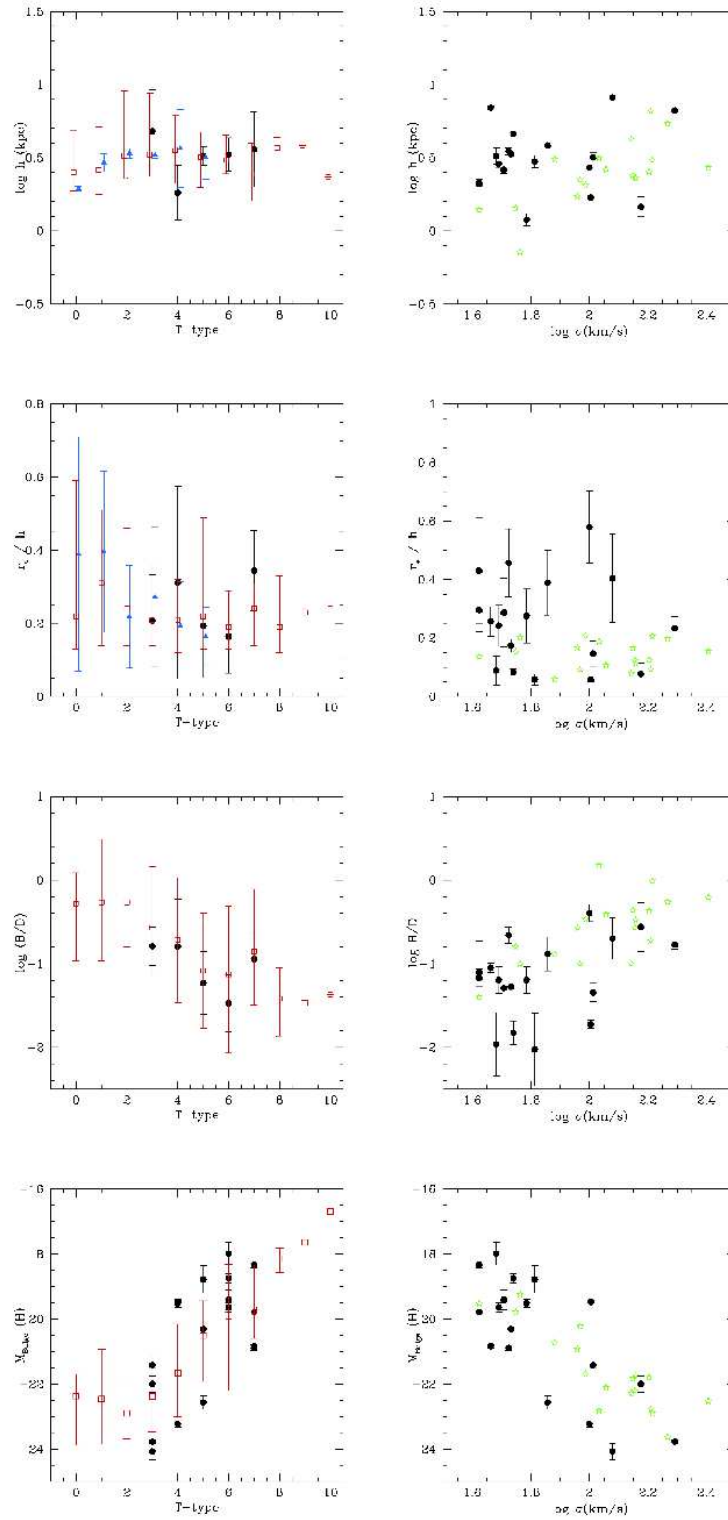


Figure B1.b. Bulge and disk structural parameters as a function of morphological T-type and central stellar velocity dispersion σ (see Fig. B1.a). *Left panels:* from top to bottom we plot disk scale length, bulge effective radius to disk scale length ratio, *H*-band bulge-to-disk ratio and bulge luminosity against T; *right panels:* same quantities plotted against $\log(\sigma)$ in km s^{-1} .

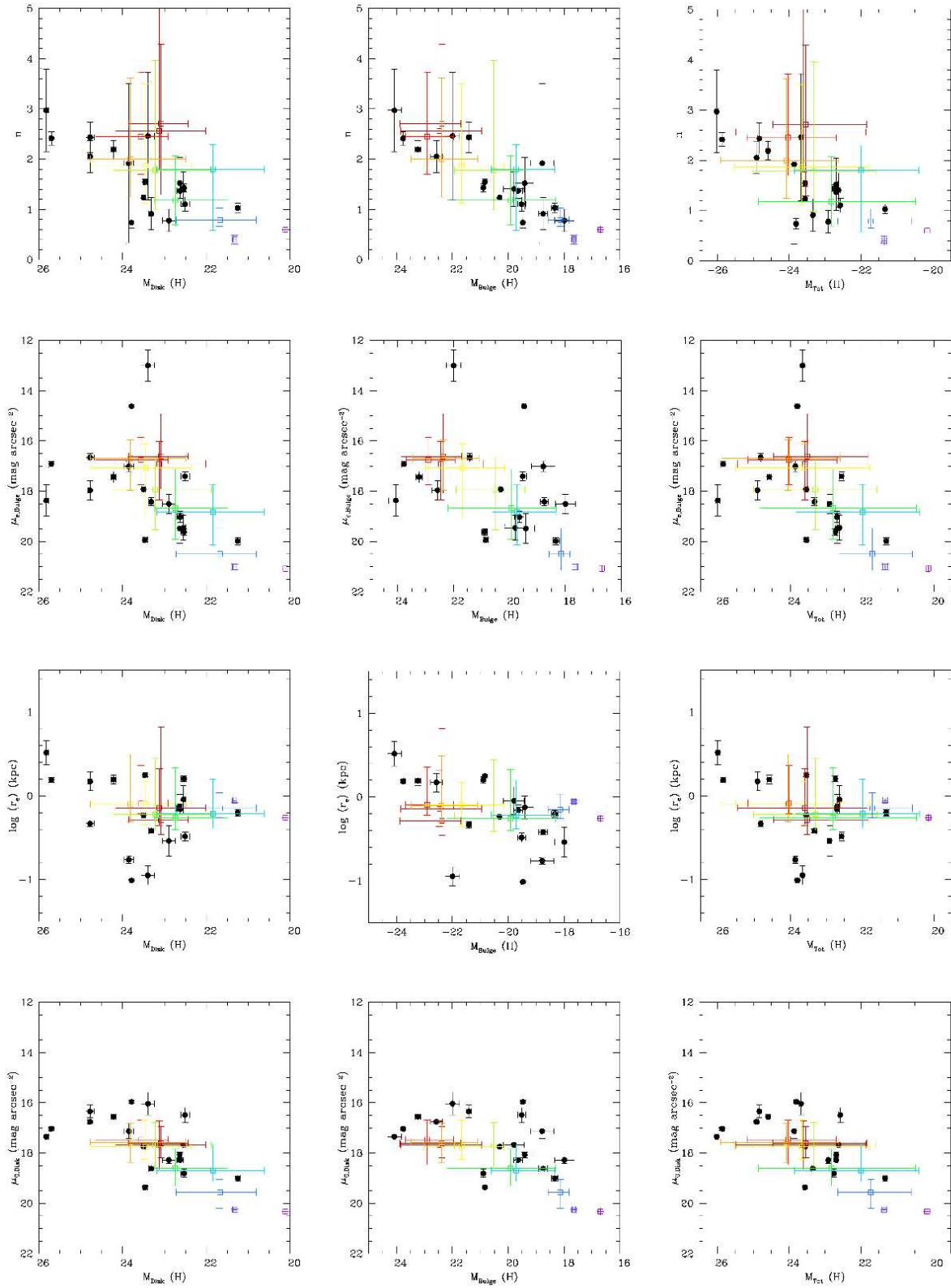


Figure B2.a. Correlations between structural parameters of bulge and disk with the luminosity of the disk (left), bulge (middle) and the whole galaxy (right). For symbols see Fig. B1.a. From top to bottom we plot correlations of Sérsic index n , bulge effective surface brightness, bulge effective radius and central disk surface brightness. The sample of Graham & Worley has been plotted in different colours, ranging from red for the earliest type galaxies to blue for the latest types.

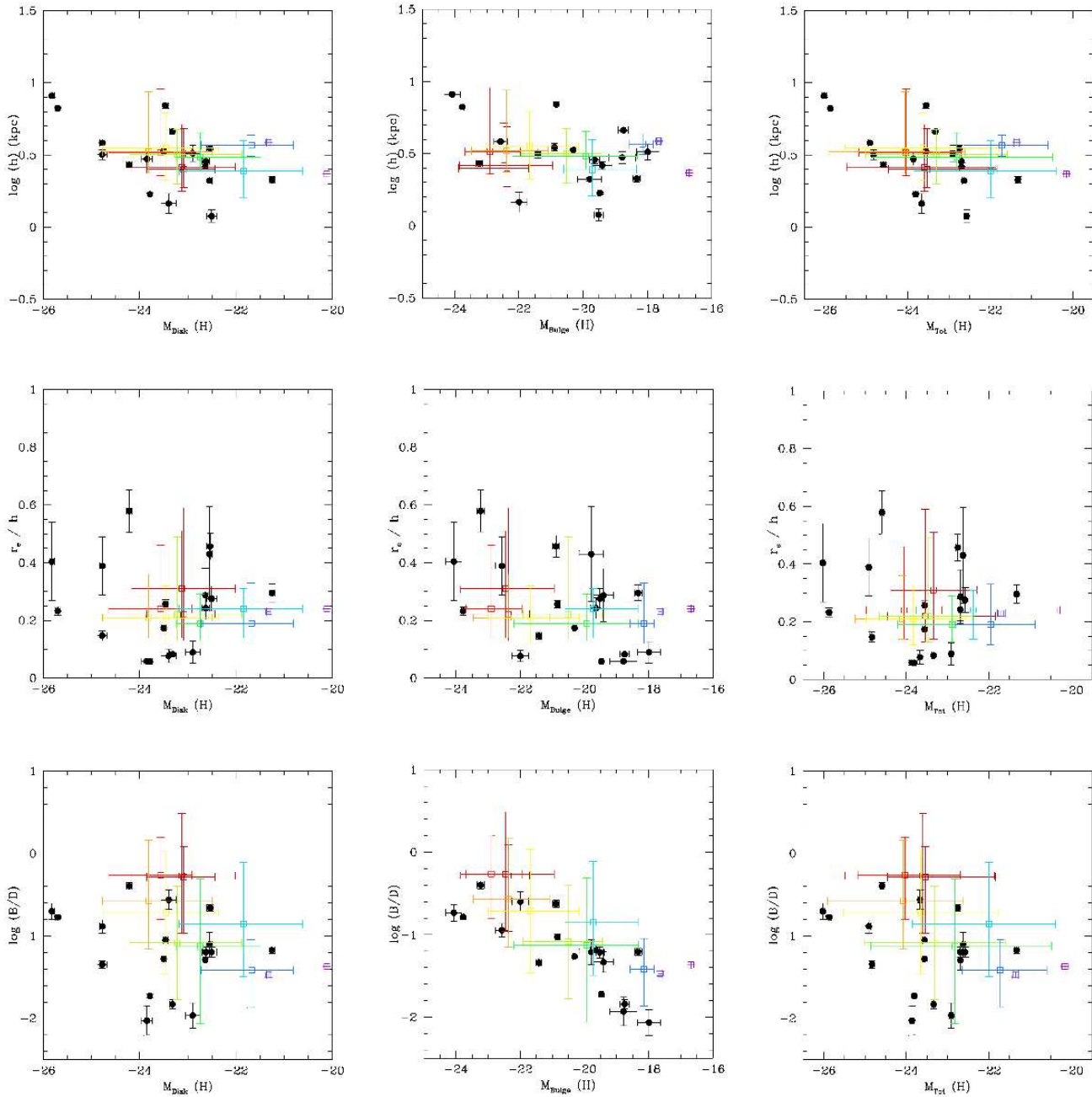


Figure B2.b. Correlations between structural parameters of bulge and disk with the luminosity of the disk (left), bulge (middle) and the whole galaxy (right). *Left panels:* from top to bottom we plot correlations with disk scale length, ratio of bulge effective radius to disk scale length, and H -band bulge-to-disk ratio. The sample of Graham & Worley has been plotted in different colours, ranging from red for the earliest type galaxies to blue for the latest types.

Peletier, R. F., & Balcells, M. 1996, *AJ*, 111, 2238

Peletier, R. F., & de Grijs, R. 1998, *MNRAS*, 300, L3

Peletier R.F. et al., 2007, *MNRAS*, 379, 445

Peletier, R. F. 2008, *Pathways Through an Eclectic Universe*, 390, 232

Phillips A.C., Illingworth G.D., MacKenty J.W., Franx M., 1996, *AJ*, 111, 1566

Pohlen M., Trujillo I., 2006, *A&A*, 454, 759

Pfenniger D., Norman C., 1990, *ApJ*, 363, 391

Popescu, C. C., Misiriotis, A., Kylafis, N. D., Tuffs, R. J., & Fischer, J. 2000, *A&A*, 362, 138

Prieto M., Aguerri J.A.L., Varela A.M., Muñoz-Tuñón C., 2001, *A&A*, 367, 405

Raha N., Sellwood J.A., James R.A., Kahn F.D., 1991, *Nature*, 352, 411

Renzini A., in 'The formation of galactic bulges', 1999, Carollo M., Ferguson H.C., Wyse R.F.G., New York - Cambridge University Press

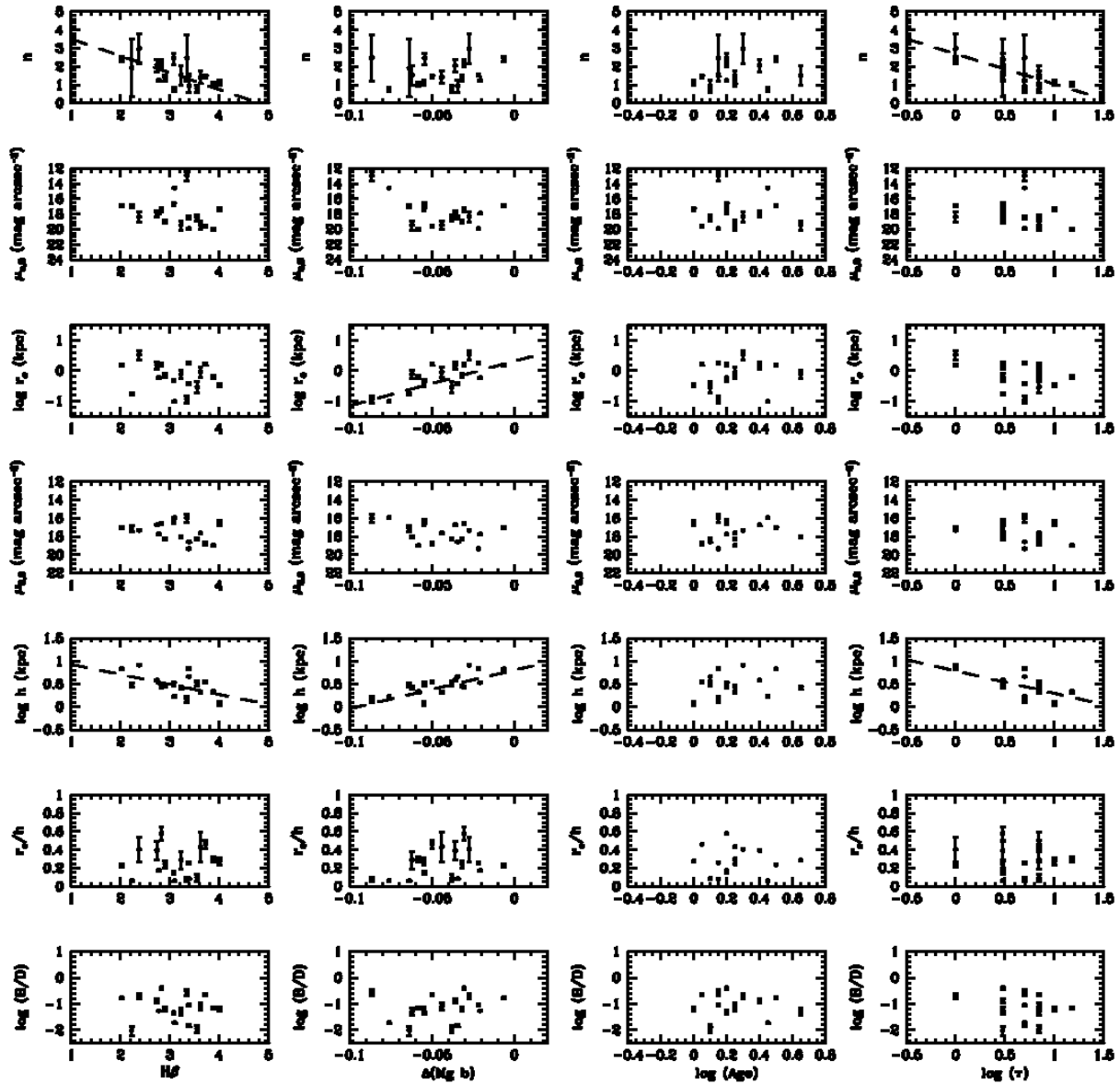


Figure B3. Correlations between the structural parameters n , $\mu_{e,b}$, r_e , $\mu_{0,Disk}$, h , r_e/h and the B/D luminosity ratio against the population parameters $H\beta$ (in Å), $\Delta Mg b'$ (in magnitudes), age and τ (in Gyr). The dashed lines overlotted in some of the panels represent a linear fit.

Rieke, G. H., & Lebofsky, M. J. 1985, *ApJ*, 288, 618
 Schombert J.M., Bothun G.D., 1987, *AJ*, 93, 60
 Seigar M.S., Carollo C.M., Stiavelli M., de Zeeuw P.T., Dejonghe H., 2002, *AJ*, 123, 184
 Sérsic J.L., 1968, *Atlas de Galaxias Australes* (Cordoba: Obs.Astronom.)
 Terndrup, D. M., Davies, R. L., Frogel, J. A., Depoy, D. L., & Wells, L. A. 1994, *ApJ*, 432, 518
 Tuffs, R. J., Popescu, C. C., Völk, H. J., Kylafis, N. D., & Dopita, M. A. 2004, *A&A*, 419, 821
 Tully, R. B., Pierce, M. J., Huang, J.-S., Saunders, W., Verheijen,

M. A. W., & Witchalls, P. L. 1998, *AJ*, 115, 2264
 Turnrose, B. E. 1976, *ApJ*, 210, 33
 Walcher, C. J., Böker, T., Charlot, S., Ho, L. C., Rix, H.-W., Rossa, J., Shields, J. C., & van der Marel, R. P. 2006, *ApJ*, 649, 692
 Wyse R.F.G., Gilmore G., Franx M., 1997, *ARA&A*, 35, 637
 Zaritsky, D., Rix, H.-W., & Rieke, M. 1993, *Nature*, 364, 313